Journal of Vertebrate Paleontology
Publication details, including instructions for authors and subscription information:
http://www.tandfonline.com/loi/ujvp20

Postcranial anatomy of Jeholosaurus shangyuanensis (Dinosauria, Ornithischia) from the Lower Cretaceous Yixian Formation of China

Feng-Lu Han [a b], Paul M. Barrett [c], Richard J. Butler [d] & Xing Xu [a]

[a] Key Laboratory of Evolutionary Systematics of Vertebrates, Institute of Vertebrate Paleontology and Paleoanthropology

[b] Graduate University of the Chinese Academy of Sciences, Chinese Academy of Sciences, 142 Xizhimenwai Street Beijing 100044, People's Republic of China

[c] Department of Earth Sciences, Natural History Museum, Cromwell Road, London, SW7 5BD, United Kingdom

[d] GeoBio-Center, Ludwig-Maximilians-Universität München, Richard-Wagner-Straße 10, Munich, D-80333, Germany

Version of record first published: 31 Oct 2012.

To cite this article: Feng-Lu Han, Paul M. Barrett, Richard J. Butler & Xing Xu (2012): Postcranial anatomy of Jeholosaurus shangyuanensis (Dinosauria, Ornithischia) from the Lower Cretaceous Yixian Formation of China, Journal of Vertebrate Paleontology, 32:6, 1370-1395

To link to this article: http://dx.doi.org/10.1080/02724634.2012.694385

Journal of Vertebrate Paleontology 32(6):1370–1395, November 2012

ARTICLE

POSTCRANIAL ANATOMY OF *JEHOLOSAURUS SHANGYUANENSIS* (DINOSAURIA, ORNITHISCHIA) FROM THE LOWER CRETACEOUS YIXIAN FORMATION OF CHINA

FENG-LU HAN,[*,1,2] PAUL M. BARRETT,[3] RICHARD J. BUTLER,[4] and XING XU[1]
[1]Key Laboratory of Evolutionary Systematics of Vertebrates, Institute of Vertebrate Paleontology and Paleoanthropology, and
[2]Graduate University of the Chinese Academy of Sciences, Chinese Academy of Sciences, 142 Xizhimenwai Street Beijing 100044, People's Republic of China; hfl0501@gmail.com; xingxu@vip.sina.com;
[3]Department of Earth Sciences, Natural History Museum, Cromwell Road, London SW7 5BD, United Kingdom; p.barrett@nhm.ac.uk;
[4]GeoBio-Center, Ludwig-Maximilians-Universität München, Richard-Wagner-Straße 10, D-80333 Munich, Germany; r.butler@lrz.uni-muenchen.de

ABSTRACT—*Jeholosaurus shangyuanensis* is a small ornithischian dinosaur from the Lower Cretaceous Yixian Formation of the Lujiatun locality, Liaoning Province, China. Here, we provide the first detailed description of its postcranial skeleton based on the holotype and four other well-preserved skeletons, and compare it with material of other primitive cerapodans. *Jeholosaurus* can be diagnosed on the basis of one postcranial autapomorphy, relating to the absence of parapophyses from the anterior dorsal vertebrae, and a unique combination of postcranial characters, but its anatomy is otherwise similar to that of many other basal ornithischians. A phylogenetic analysis incorporating these new postcranial data confirms previous suggestions that *Jeholosaurus* is a basal ornithopod and that it forms a clade with *Changchunsaurus* and *Haya*; *Koreanosaurus* and *Yueosaurus* might also belong to this clade, though additional material of both will be required to test this hypothesis. The name Jeholosauridae is proposed for this apparently endemic group of Cretaceous East Asian taxa.

INTRODUCTION

Phylogenetic relationships among basal ornithopod dinosaurs are poorly understood and the published tree topologies for these taxa, and other basal cerapodans, have only weak statistical support (e.g., Xu et al., 2006; Butler et al., 2007, 2008). This problem stems from a number of causes, including the fragmentary remains of many of the specimens and the difficulties in finding characters with strong enough phylogenetic signals to tease apart the early evolutionary history of the clade. The first step needed to improve this situation is the provision of more detailed information on the anatomy of basal ornithopods, in order to highlight potential characters that might be of phylogenetic significance.

Jeholosaurus shangyuanensis is a small ornithischian dinosaur from the Lower Cretaceous Yixian Formation of Lujiatun, Liaoning Province, China (Xu et al., 2000). Xu et al. (2000) provided a preliminary description of two specimens, the holotype (IVPP V12529, a skull and associated partial postcranial specimen) and one referred specimen (IVPP V12530, a skull with associated cervical vertebrae), and assigned this taxon to a basal position within Ornithopoda. Subsequently, a detailed description of the cranial anatomy was produced on the basis of these specimens and four other nearly complete skulls (Barrett and Han, 2009). Interestingly, *Jeholosaurus* was shown to possess a combination of features present in both ornithopods and marginocephalians, making attribution to either one of these clades difficult (Barrett and Han, 2009). Nevertheless, all previous phylogenetic analyses that include *Jeholosaurus* have generally recovered it as a basal ornithopod (Xu et al., 2000; Butler et al., 2008; Barrett and Han, 2009), often in a clade with *Changchunsaurus* from the Quantou Formation (Aptian–Cenomanian) of Jilin Province, China (Butler et al., 2011), and *Haya griva* from the Javkhlant Formation (?Santonian) of Mongolia (Makovicky et al., 2011). By contrast, an alternative proposal is that *Jeholosaurus* and *Changchunsaurus* might be basal marginocephalians, on the basis of an as yet unpublished phylogenetic analysis that incorporated information from seven individuals of *Jeholosaurus*, including five nearly complete skeletons (Han, 2009). Here, we provide the first detailed postcranial description of *Jeholosaurus shangyuanensis*, based on the holotype specimen, the original referred specimen, and three other nearly complete postcranial specimens, and assess the impact of this new information on the systematics of basal cerapodans.

Institutional Abbreviations—**IVPP**, Institute of Vertebrate Paleontology and Paleoanthropology, Beijing; **NHMUK**, Natural History Museum, London; **SAM**, Iziko South African Museum, Cape Town; **ZDM**, Zigong Dinosaur Museum, Zigong.

SYSTEMATIC PALEONTOLOGY

DINOSAURIA Owen, 1842
ORNITHISCHIA Seeley, 1887
CERAPODA Sereno, 1986, sensu Butler et al. (2008)
ORNITHOPODA Marsh, 1881, sensu Butler et al. (2008)
JEHOLOSAURIDAE, fam. nov.

Diagnosis—All ornithischians more closely related to *Jeholosaurus shangyuanensis* Xu, Wang, and You, 2000, than to *Hypsilophodon foxii* Huxley, 1869, *Iguanodon bernissartensis* Boulenger in Beneden, 1881, *Protoceratops andrewsi* Granger and Gregory, 1923, *Pachycephalosaurus wyomingensis* (Gilmore, 1931), or *Thescelosaurus neglectus* Gilmore, 1913.

Type Species—*Jeholosaurus shangyuanensis* Xu, Wang, and You, 2000.

Taxonomic Content—*Jeholosaurus shangyuanensis* Xu, Wang, and You, 2000, *Haya griva* Makovicky, Kilbourne, Sadleir, and

*Corresponding author.

Norell, 2011, and *Changchunsaurus parvus* Zan, Chen, Jin, and Li, 2005.

JEHOLOSAURUS Xu, Wang, and You, 2000

Type Species—*Jeholosaurus shangyuanensis* (by monotypy).

Diagnosis—As for the type species (see below).

Distribution—Early Cretaceous (?upper Barremian–lower Aptian), northeastern China.

JEHOLOSAURUS SHANGYUANENSIS Xu, Wang, and You, 2000
(Figs. 1–13)

Emended Diagnosis—Cranial autapomorphy: presence of a row of small foramina on the lateral surface of the nasal immediately dorsal to the premaxillary articulation. Unique combination of cranial character states: six premaxillary teeth (distinct from all other cerapodans, but present in *Lesothosaurus*, *Scutellosaurus*, and some ankylosaurs); presence of a foramen enclosed within the quadratojugal (distinct from all ornithischians except *Haya*, *Hypsilophodon*, and *Tenontosaurus*); combined presence of nodular ornamentation on the postorbital and jugal (distinct from all ornithopods and non-cerapodan ornithischians, but also present in pachycephalosaurs, *Archaeoceratops*, *Xuanhuaceratops*, and *Yinlong*); and jugal caudal process bifurcated distally (distinct from all cerapodans except *Psittacosaurus*, but present in some early ornithischians including *Emausaurus*, *Lesothosaurus*, and *Scelidosaurus*). Cranial characters are discussed in detail in Barrett and Han (2009).

Postcranial autapomorphy: parapophyses absent from dorsal vertebrae 1 and 2. Unique combination of postcranial character states: possession of three distal tarsals, with fused distal tarsals 1 and 2 (distinct from all other ornithischians, with the exception of *Orodromeus*) and phalanx 3–4 is the longest element in pedal digit 3 (also present in *Xiaosaurus*).

Holotype—IVPP V12529, a partial skeleton consisting of a skull, seven cervical vertebrae, several fragmentary dorsal vertebrae and partial sacrum, articulated sections of caudal vertebrae, and both hind limbs.

Locality and Horizon—Lujiatun, Liaoning Province, People's Republic of China; 'Lujiatun Bed,' Yixian Formation, ?upper Barremian–lower Aptian, Early Cretaceous (Wang et al., 1998; He et al., 2006). The locality is collection number 53493 within the Paleobiology Database. It is not known if all of the specimens are from the same level within the 'Lujiatun Beds' and this seems unlikely given the preservational differences between them. However, they were all recovered from the complex of sites around Lujiatun that pertain to the 'Lujiatun Beds.'

Referred Specimens—IVPP V12530, a skull with articulated cervical vertebrae; IVPP V12542, a skull with a nearly complete vertebral column, partial forelimb and hind limb, and a nearly complete pelvis; IVPP V15719, a nearly complete skull, partial axial column, pelvic girdle, and hind limbs; IVPP V15939, partial post-cervical axial column, partial pelvic girdle, and a complete hind limb and pes.

Material—Four of the five specimens described herein are associated with skulls (IVPP V12529, V12530, V12542, and V15719), allowing them all to be referred to *Jeholosaurus* on the basis of diagnostic cranial characters (Barrett and Han, 2009). The fifth specimen (IVPP V15939), which is also the largest, consists only of postcranial elements, but shares the diagnostic combination of postcranial characters present in the other specimens.

IVPP V12529. Postcranial elements of the holotype specimen include the anterior cervical vertebrae (cervicals 1–7, which are well preserved); four strongly compressed anterior dorsal vertebrae; three associated, but badly damaged sacral vertebrae; several groups of well-preserved, articulated caudal vertebrae (whose exact positions within the tail cannot be determined with confidence); the almost complete left femur and the distal part of the right femur; both tibiae and fibulae; the right astragalus (which is broken and preserved in two sections: one in articulation with the right tibia, and the other in articulation with the right pes), the ascending process of the left astragalus, and both calcanea; and substantial portions of both feet, which are well preserved, but somewhat compressed mediolaterally (see Xu et al., 2000).

IVPP V12530. The only postcranial elements preserved in this specimen are 10 articulated vertebrae, consisting of the axial neural arch (the axial centrum and axis are not preserved), cervicals 3–9, and dorsals 1–2.

IVPP V12542. A previously undescribed partial skeleton consisting of a damaged, but almost complete skull; an articulated vertebral column extending from the middle of the dorsal series to the middle of the tail, including a complete sacrum and several chevrons, but lacking dorsal and caudal ribs; a right humerus; pelvic girdle elements (articulated ischium and pubis and displaced ilium); right and left femora and tibiae; a right fibula; and a left pes. The specimen is still embedded in matrix and all of the elements are visible from one side only.

IVPP V15719. This is the smallest specimen in the sample and remains partially embedded within a white tuffaceous mudstone block. Consequently, many of the elements are visible in one view only. The preserved parts of the skeleton are generally articulated, though the right forelimb and the anterior–middle parts of the dorsal vertebral column, and most of the tail, are missing. In addition to the skull, IVPP V15719 consists of a series of articulated cervical/dorsal vertebrae (from the axis to dorsal 1); a left scapula, coracoid, and humerus; a section of vertebral column comprising five dorsal vertebrae and three sacral vertebrae; five caudal vertebrae; an almost complete right ilium and right ischium, the proximal end of the right pubis, and a damaged left ischium (missing the central part of its shaft); left and right femora (left femur complete, right femur represented by the distal end only), tibiae (both complete), and fibulae (distal part only on the left side); the right astragalus and calcaneum; and partial left and right pedes. An isolated metatarsal preserved in the block represents another larger animal and will not be discussed further herein.

IVPP V15939. This specimen represents the largest known individual and is well preserved. It includes a set of four associated dorsal vertebrae, one isolated dorsal, an articulated vertebral column extending from the posterior-most dorsal through the sacrum to caudal vertebra 9; both ilia and ischia, an almost complete right pubis and the left pubic shaft, with most of the girdle elements in articulation with each other and the sacrum; and complete left and right hind limbs.

None of the specimens includes a complete dorsal or caudal vertebral series, sterna, ulnae, radii, or manual elements. Key measurements from all of these specimens are provided in Appendix 1.

Comments—Xu et al. (2000) included three postcranial characters in their diagnosis of *Jeholosaurus*, but none of these are autapomorphic. The first of these, absence of an anterior intercondylar groove on the distal femur, is an ornithischian symplesiomorphy (e.g., Butler et al., 2008). The second, the tubular arrangement of the metatarsals, is due to preservational factors affecting the holotype specimen (IVPP V12529) and is not present in any of the better-preserved referred specimens (e.g., IVPP V15939). Finally, pedal phalanx 3–4 is the longest phalanx in pedal digit 3 not only in *Jeholosaurus*, but also in *Xiaosaurus*, as noted by Xu et al. (2000). However, this does form part of a unique character combination for *Jeholosaurus* (see Diagnosis, above). The proposed autapomorphy and unique combination of characters proposed herein are visible in the holotype specimen and can also be seen in some of the referred specimens, notably IVPP V15939, which lacks an associated skull and whose referral

to *Jeholosaurus* relies on postcranial characters alone. Additional discussion of these features is provided below.

DESCRIPTION AND COMPARISONS

Axial Skeleton

Cervical Series—The cervical vertebrae can be completely reconstructed on the basis of IVPP V12529, IVPP V12530, and IVPP V15719 (Figs. 1, 2). *Jeholosaurus* possessed a total of nine cervical vertebrae, as also occurs in *Heterodontosaurus* (SAM-PK-K1332; Santa Luca, 1980), ?*Scutellosaurus* (Colbert, 1981), the basal neornithischians *Hexinlusaurus* (ZDM T6001; He and Cai, 1984; Barrett et al., 2005) and *Agilisaurus* (ZDM T6011; Peng, 1992), non-iguanodontian ornithopods (e.g., *Changchunsaurus* [Butler et al., 2011], *Haya* [Makovicky et al., 2011], *Hypsilophodon* [NHMUK R196; Galton, 1974], and *Orodromeus* [Scheetz, 1999]), and most species of the basal ceratopsian *Psittacosaurus* (Russell and Zhao, 1996; You and Dodson, 2004). Fewer cervical vertebrae occur in the basal thyreophoran *Scelidosaurus* (six cervicals; NHMUK R1111; Owen, 1863; Norman et al., 2004a), ankylosaurs (seven to eight cervicals; Vickaryous et al., 2004), and the early stegosaur *Huayangosaurus* (eight cervicals; Zhou, 1984), whereas more than nine cervical vertebrae appear in iguanodontian ornithopods (Norman, 2004) and most ceratopsians (Dodson et al., 2004; You and Dodson, 2004). Cervical vertebrae 1–7 are preserved in the holotype (Fig. 1A, C–F) and cervical vertebrae 2–9 are present in IVPP V12530 (Fig. 1B) and IVPP V15719 (Fig. 2).

Atlas—The proatlas is not preserved in any of the available specimens and the only information available for the atlas comes from the holotype (IVPP V12529), which includes the atlantal intercentrum and right atlantal neural arch only (Fig. 1). The atlantal intercentrum has rotated to the left relative to its life position (Fig. 1A, D). In anterior view, the intercentrum has a crescentic outline (Fig. 1D). Its anterior surface slopes posterodorsally and is concave for the reception of the occipital condyle. This fossa is deepest on the midline and becomes shallower laterally. A distinct, thin flange forms the ventral margin of the fossa and separates the anterior surface of the intercentrum from its ventral surface. In anterior view, the lateral margins of the intercentrum are dorsoventrally expanded; the dorsal margins of these expansions form the articular regions for the atlantal neural arches, whereas the ventral parts form ventrolaterally extending bosses (diapophyses) that would have articulated with the atlantal ribs. These bosses are present in *Hypsilophodon* (NHMUK R2477; Galton, 1974), but are only

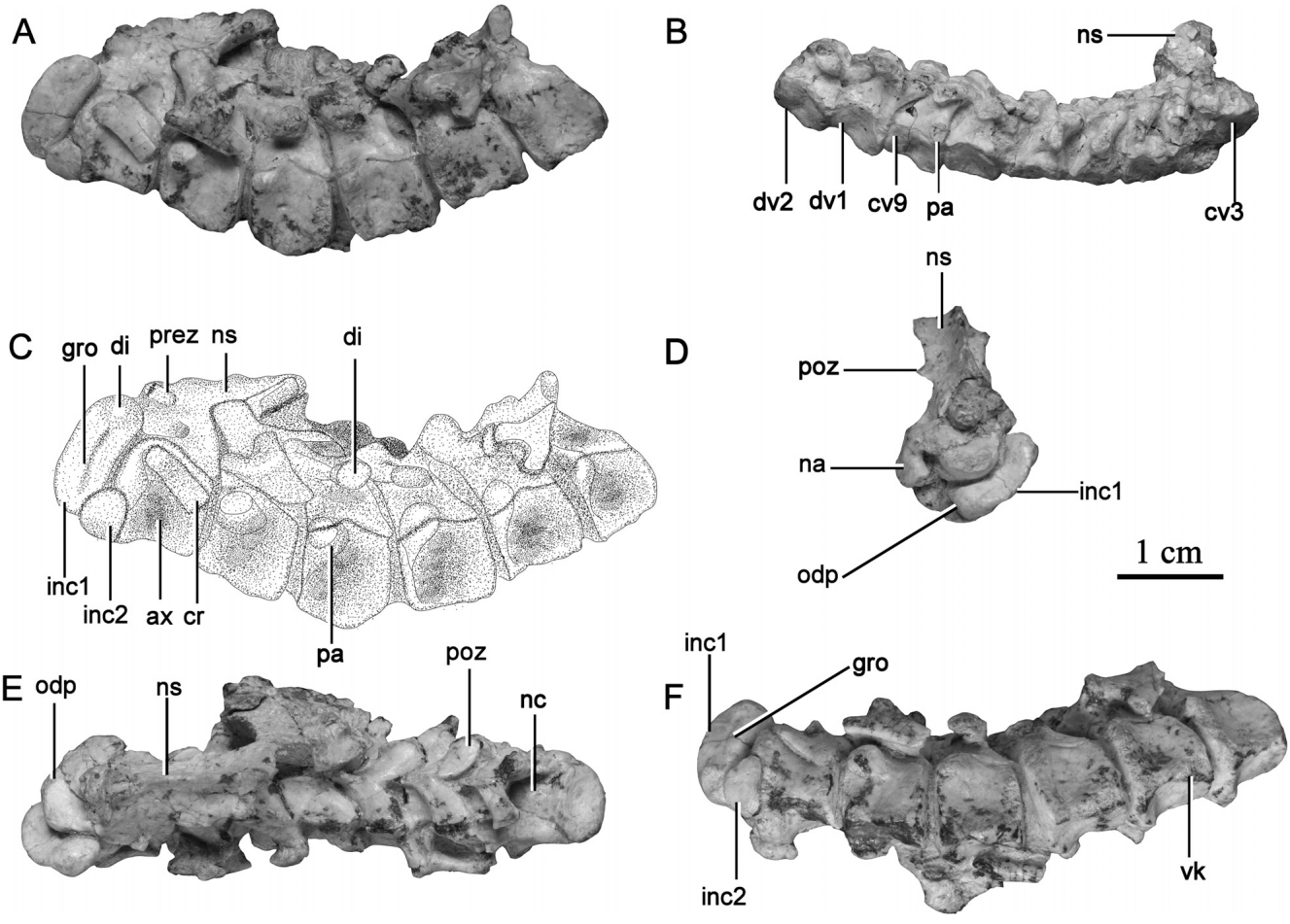

FIGURE 1. Photographs and outline drawing of the cervical vertebrae of *Jeholosaurus shangyuanensis* (IVPP V12529 and IVPP V12530). **A**, cervical vertebrae 1–7 of the holotype IVPP V12529 in left lateral view; **B**, cervical vertebrae 2–9 (note only the neural spine of the axis is preserved) and anterior dorsal vertebrae 1–2 of IVPP V12530 in right lateral view. Note the absence of parapophyses on dorsals 1 and 2; **C**, outline drawing of cervical vertebrae 1–7 of IVPP V12529 in left lateral view; **D**, atlas-axis of IVPP V12529 in anterior view; **E**, cervical vertebrae 1–7 of IVPP V12529 in dorsal view; **F**, Cervical vertebrae 1–7 of IVPP V12529 in ventral view. **Abbreviations**: **ax**, axis; **cr**, cervical rib; **cv**, cervical vertebrae; **di**, diapophysis; **dv**, dorsal vertebrae; **gro**, groove; **inc1**, atlas intercentrum; **inc2**, axis intercentrum; **na**, neural arch; **nc**, neural canal; **ns**, neural spine; **odp**, odontoid process; **pa**, parapophysis; **poz**, postzygapophysis; **prez**, prezygapophysis; **vk**, ventral keel.

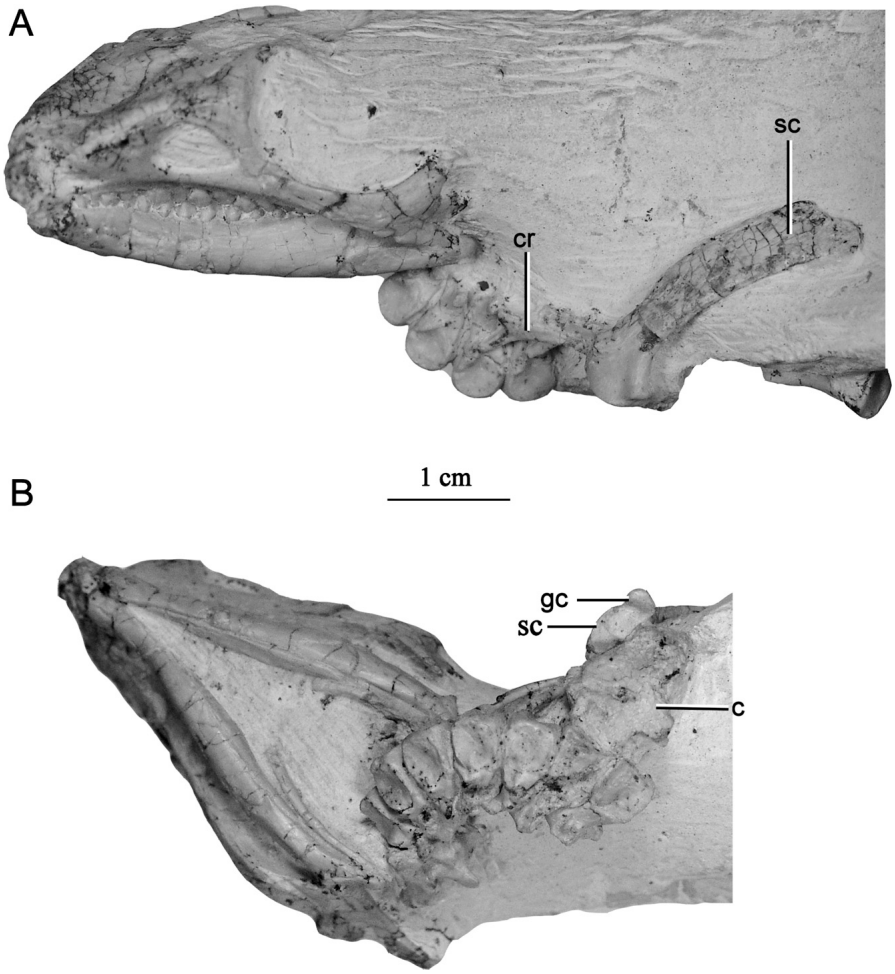

FIGURE 2. Skull, neck, and pectoral girdle of *Jeholosaurus shangyuanensis* (IVPP V15719). **A**, lateral view; **B**, ventral view. **Abbreviations**: **c**, coracoid; **cr**, cervical rib; **gc**, glenoid cavity; **sc**, scapula.

subtly developed in *Hexinlusaurus* (ZDM T6001; He and Cai, 1984). In ventral view, the intercentrum is anteroposteriorly narrow and the surface is excavated with a broad groove that is delimited by the anterior and posterior margins of the intercentrum and the diapophyses (Fig. 1A, C). A similar groove is present in *Hexinlusaurus* (He and Cai, 1984). In lateral view, the intercentrum is wedge-shaped, being broadest centrally and tapering to a narrow dorsal apex. The posterior surface of the intercentrum is partially obscured by the axis, but the visible portion shows that it was shallowly convex.

The right neural arch (Fig. 1D) has become disarticulated from the intercentrum and forms an inverted 'L'-shape in anterior and lateral views. The postzygapophysis is missing and the prezygapophysis is damaged anteriorly. In lateral view, the base of the neural arch is expanded to form the articulation with the intercentrum, but the arch narrows as it extends dorsally, before expanding again to form the pre- and postzygapophyses (Fig. 1A, C). Ventrally, the articular surface for the intercentrum is anteroposteriorly and mediolaterally expanded and rugose. An angle of approximately 90° separates the long axis of the neural arch pedicle from the prezygapophysis.

Axis—The axis is well preserved and essentially complete in IVPP V12529 (Fig. 1A, C–F), the axial neural arch is present in IVPP V12530 (Fig. 1B), and IVPP V15719 includes the axial centrum. As a result, the following description is based primarily on IVPP V12529, supplemented with information from the other two specimens. The various components of the axis in IVPP V12529 have not fused, and the junctions between the centrum, intercentrum, and neural arch are clearly visible. It is not possible to determine whether the odontoid is fused to the centrum or not as its contacts are obscured.

In anterior view, the odontoid process is prominent, with a hemispherical outline and strongly convex articular surface (Fig. 1D). The subrounded ventral surface is in articulation with the intercentrum. In dorsal view, the dorsal surface of the odontoid process is planar and has a convex anterior margin (Fig. 1E). The anterior and posterior surfaces of the centrum are flat, and semicircular in outline. The lateral surfaces of the centrum are excavated so that they are strongly concave anteroposteriorly and convex dorsoventrally; the two surfaces converge ventrally to form a sharp keel that gives the centrum a triangular transverse cross-section at midlength. By contrast, the axial centrum of *Haya* lacks a distinct keel (Makovicky et al., 2011). Anteriorly, the centrum articulates with a small, wedge-shaped intercentrum. There is no trace of any foramina on the lateral surface of the axis. A prominent, dorsoventrally elongate parapophysis is present at the junction of the anterior edge and lateral margins of the centrum at approximately midheight (Fig. 1A, C).

The height of the neural arch is slightly greater than that of the centrum. Laterally, it supports a slender, finger-like diapophysis that is positioned just dorsal to the neurocentral suture. The presence of an axial diapophysis contrasts with the condition in *Changchunsaurus* in which the diapophysis is absent (Butler et al., 2011). Prezygapophyses were present, but are not well

preserved, and only the base of the left prezygapophysis is visible in IVPP V12529 (Fig. 1C). The postzygapophyses are positioned slightly more dorsally on the arch than the prezygapophyses and face ventrolaterally; in IVPP V12529 they are in articulation with the prezygapophyses of cervical 3. In lateral view, the neural spine is oriented posterodorsally at an angle of 45° to the horizontal and in anterior view it is expanded transversely to form a vaulted plate (Fig. 1A, C, E). The midline of the spine forms a sharp crest that extends along its entire length. The neural spine is very elongate and extends beyond the posterior margin of the axial centrum to overlap cervical vertebra 3 (Fig. 1A, C), as occurs in some early ornithischians, including *Lesothosaurus* (Sereno, 1991) and *Heterodontosaurus* (Santa Luca, 1980), non-iguanodontian ornithopods, such as *Haya* (Makovicky et al., 2011) and *Changchunsaurus* (Butler et al., 2011), and some ceratopsians (Butler et al., 2011). Breakage to the axial neural spine in IVPP V12530 results in a structure on the right-hand side that resembles a strongly developed epipophysis, whose presence would be unusual in an ornithischian; however, this feature is actually the result of damage to the spine and a similar process is not present on the left-hand side.

An axial rib is preserved in IVPP V12529. It is short, but broken distally, and its proximal end is in contact with the parapophysis. The dorsal part of the rib is damaged, so it is not possible to confirm the presence or absence of a second rib head, but the presence of a diapophysis suggests that the rib may have been at least incipiently double-headed.

Cervical Vertebrae 3–9—The centra of cervicals 3–9 are amphiplatyan to slightly amphicoelous (Figs. 1, 2). They are pentagonal and shield-shaped in anterior or posterior view, and have anteroposteriorly concave, saddle-shaped lateral surfaces that each bear a small centrally positioned nutrient foramen. All of the cervicals possess thin, sharp keels on the ventral midline (Fig. 1F); similar keels are present in basal ornithischians, including *Heterodontosaurus* (Santa Luca, 1980), *Stormbergia* (Butler, 2005), *Eocursor* (Butler, 2010), and *Hexinlusaurus* (He and Cai, 1984), and some basal ornithopods, such as *Changchunsaurus* (Butler et al., 2011) and *Orodromeus* (Scheetz, 1999). These ventral keels differ from those in some other ornithopods (e.g., *Hypsilophodon*: NHMUK R196; Galton, 1974) and basal ceratopsians (e.g., *Psittacosaurus*: Averianov et al., 2006), which have much broader keels.

In lateral view, all of the centra have an almost square outline, with subequal dorsoventral heights and anteroposterior widths, and they are also similar in length to each other along the entire cervical column (Fig. 1A–C). This combination of features also occurs in *Changchunsaurus* (Butler et al., 2011), *Orodromeus* (Scheetz, 1999), *Psittacosaurus* (Averianov et al., 2006), and *Yueosaurus* (Zheng et al., 2012), but differs from the condition in *Heterodontosaurus* (SAM-PK-K1332; Santa Luca, 1980), *Hexinlusaurus* (He and Cai, 1984), and *Hypsilophodon* (NHMUK R196; Galton, 1974), and especially *Koreanosaurus* (Huh et al., 2010) in which the cervical centra are significantly longer than tall. As in *Changchunsaurus*, *Haya*, and several other basal cerapodans, the ventral margins of the anterior cervical centra are slightly convex in lateral view, rather than concave or straight as in the majority of other ornithischians, such as *Heterodontosaurus*, *Hypsilophodon*, *Orodromeus*, *Psittacosaurus*, and *Yueosaurus* (Butler et al., 2011; Makovicky et al., 2011; Zheng et al., 2012).

The parapophyses are stout rounded processes, with subovate outlines in lateral view. In IVPP V12529, cervical 3 bears dorsolaterally extending parapophyses that are positioned at the anterodorsal corner of the centrum, just ventral to the neurocentral junction. Between cervical vertebrae 4–7 the parapophyses migrate dorsally to straddle the neurocentral suture, with the articular surface of the parapophysis now facing anteroventrally (Fig. 1A–C). In IVPP V12530 and IVPP V15719, the majority of the parapophysis lies above the suture in cervical vertebra 9 (Fig. 1B). The dorsolateral orientation of the parapophyses in *Jeholosaurus* differs from the ventrolateral orientation present in *Yueosaurus* (Zheng et al., 2012). The sutures between the neural arch and centrum are not straight, but ascend dorsally to reach its highest point at a point approximately halfway along the centrum before descending ventrally to the posterior margin of the vertebra.

The neural arches become progressively taller through cervicals 3–7, as in other ornithischians. In IVPP V12529, the posteroventrally extending diapophyses of cervical 3 are much more robust and elongate than those of the axis. The diapophyses remain similar in shape along the cervical series. They have cylindrical cross-sections and project posteroventrally, forming an angle of approximately 45° with the horizontal in both lateral and dorsal views. In IVPP V12530 and IVPP V15719, the position of the diapophysis migrates dorsally in more posterior cervicals and the direction in which they extend from the neural arch gradually changes from posteroventral to more posterolateral. In dorsal view, the distal end of the diapophysis in cervical 3 is slightly expanded anteroposteriorly relative to its shaft. However, this distal expansion is not present, or is only very weakly developed, in the other cervical vertebrae. In IVPP V12530, the diapophyses become progressively longer posteriorly, so that cervical 8 has the longest and most robust diapophysis in the neck, as preserved (Fig. 1B).

In all cervical vertebrae, the neural arches are inclined slightly anteriorly in lateral view. The neural spine of cervical 3 is relatively prominent, as in *Changchunsaurus* and *Haya*, in contrast to the small neural spines present on the cervical 3 of other small ornithischians (Fig. 1A, C; Butler et al., 2011; Makovicky et al., 2011). The remaining cervical neural spines are lower in height and are transversely compressed plates, whose summit forms a sharp ridge dorsally. In posterior view, the neural canals are broad and ovate in outline, narrowing dorsally. The prezygapophyses face dorsomedially and have facets oriented at an angle of approximately 30° to the vertical, whereas the postzygapophyses face ventrolaterally. As the cervicals in all specimens are preserved in articulation, other features of the pre- and postzygapophyses are generally obscured. Nevertheless, as in the majority of small ornithischians (e.g., Galton, 1974; Scheetz, 1999), the postzygapophyses appear to be relatively short, and do not overlap the succeeding vertebra for a considerable distance, in contrast to the elongate postzygapophyses present in *Koreanosaurus* (Huh et al., 2010).

In cervical 7 of IVPP V12529, a short lamina forms the medioventral border of a posteriorly opening, shallow fossa that is bounded dorsomedially by the postzygapophysis, dorsally by a low postzygodiapophyseal lamina, and laterally by an incipient posterior centrodiapophyseal lamina. This fossa is also present in an incipient form on cervical 6 of the same specimen.

Incomplete cervical ribs, consisting of the proximal part only, are present in IVPP V12529 (Fig. 1A, C), whereas in IVPP V15719 only the seventh and eighth cervical ribs are preserved (Fig. 2A). The post-axial cervical ribs are double-headed. The anterior cervical ribs are more slender than those on more posterior cervicals. They are 'Y'-shaped in lateral view, but the tuberculum is longer and more slender than the capitulum. The capitulum and tuberculum form an angle of approximately 90° and the rib shaft tapers distally.

Dorsal Vertebrae—Dorsal vertebrae are partially preserved in most of the above-mentioned specimens, but none of these preserve a complete dorsal series. It is likely that the complete dorsal column contained around 15 vertebrae, based on comparisons with other closely related taxa, such as *Hypsilophodon* (Galton, 1974). The first dorsal vertebra and dorsal vertebrae 1 and 2 are present in IVPP V15719 and IVPP V12530, respectively, preserved in articulation with the neck, and are similar

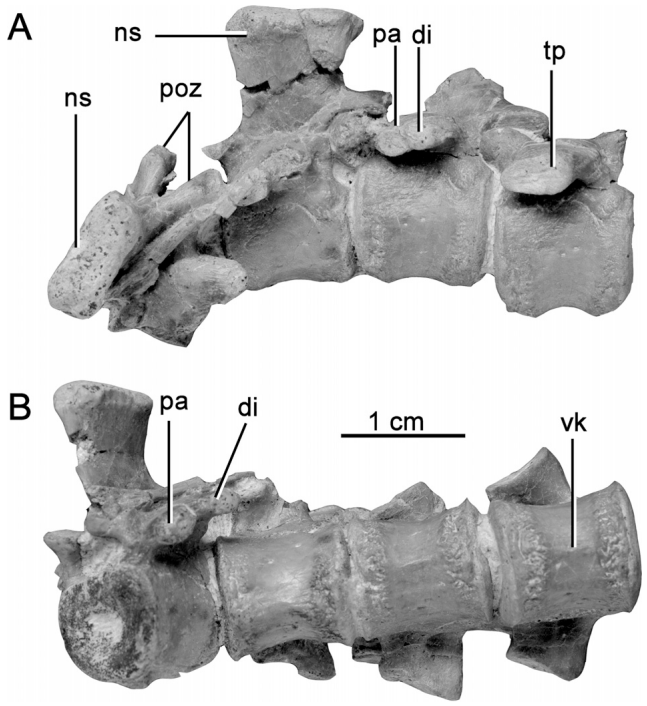

FIGURE 3. The last four dorsal vertebrae of *Jeholosaurus shangyuanensis* (IVPP V15939). **A**, left lateral view; **B**, ventral view. **Abbreviations**: **di**, diapophysis; **ns**, neural spine; **pa**, parapophysis; **poz**, postzygapophysis; **tp**, transverse process; **vk**; ventral keel.

to the cervicals (Figs. 1B and 2B). IVPP V15939 includes six dorsal vertebrae: four in articulated series and the fifth and sixth articulated with the sacrum in a separate block (Figs. 3, 4). The last five dorsals are also preserved in articulation with the sacrum in IVPP V15719. Ten dorsal vertebrae are preserved in IVPP V12542, but their surfaces are badly damaged and provide little information about their anatomy (Fig. 5A).

All of the preserved dorsal vertebrae are slightly amphicoelous. The anterior dorsals are very similar to the posterior cervicals and differ from the posterior dorsals in several respects. Dorsals 1 and 2 lack parapophyses (Fig. 1B), whereas these structures are well developed on the posterior dorsals (Fig. 3). By contrast, parapophyses are present on dorsals 1 and 2 in other small ornithischians (e.g., *Hexinlusaurus* [He and Cai, 1984], *Hypsilophodon* [Galton, 1974], and *Orodromeus* [Scheetz, 1999]; the condition cannot be determined in *Changchunsaurus* or *Haya* due to preservation [Butler et al., 2011; Makovicky et al., 2011]) and their absence is provisionally regarded as an autapomorphy of *Jeholosaurus*. In addition, the posterior articular surfaces of the anterior dorsal centra have a subpentagonal outline, whereas those of the posterior dorsals are subcircular. This difference is due to the presence of a sharp, midline ventral keel on the anterior dorsals (IVPP V12530, IVPP V15719; Fig. 1B), which develops into a small process on the ventral midline of the anterior articular surface and is absent from the posterior dorsals (see below).

In anterior or posterior view, the posterior dorsal centra are approximately as wide as they are high (Figs. 3, 4, and 6; IVPP V15719 and IVPP V15939). The lateral surfaces are depressed relative to the articular regions and are gently concave longitudinally. Very small nutrient foramina are present in the center of this depression, and are variable in number, size, and exact position (Fig. 3). The ventral surface is broad and divided from the lateral surfaces by subtle breaks in slope, rather than well-defined ridges. Each ventral surface bears a distinct, but low, midline keel, which is more strongly developed in the posterior-most dorsals than in the middle dorsals (Fig. 3). Immediately adjacent to the articular surfaces, the lateral and ventral margins of the centra are textured with numerous fine grooves and pits, which are obvious on IVPP V15939 (Fig. 3), but hard to see in IVPP V15719 and IVPP V12542. In IVPP V15939 and IVPP V15719, the neurocentral sutures are open.

In all of the posterior dorsals, the neural canals are subelliptical in outline and are broader than they are high (visible in IVPP V15939 only). The transverse processes have a 'stepped' morphology in dorsal view, with the diapophysis extending further laterally than the parapophysis. The parapophysis and diapophysis are situated at almost the same height in lateral view. In anterior or posterior view, the transverse processes extend almost horizontally, and a little posteriorly, and thicken dorsoventrally towards their lateral ends. In the posterior-most dorsals, the parapophysis coalesces with the diapophysis, so that in the first two preserved dorsals of IVPP V15939 (dorsals 10–11, assuming a total dorsal count of 15) these processes are still distinct, but are joined to form a compound articular surface with a horizontally oriented 'figure-of-eight'-shaped outline in lateral view (Fig. 3A). Posterior to this point (dorsals 12–15) the stepped morphology of the transverse process disappears to replaced by a simpler morphology with subparallel anterior and posterior margins. The parapophysis and diapophysis merge in these vertebrae to form a single undivided articular surface.

In ventral view, the transverse processes bear a ridge that subdivides the ventral surface into two depressions, which extend along the anteroventral and posteroventral surfaces of the process respectively. Dorsally, the surface of transverse process is gently convex anteroposteriorly.

The transverse processes lie at nearly the same level as the zygapophyses. The articular surfaces of the prezygapophyses face dorsomedially at an angle of 45° to the horizontal, whereas those of the postzygapophyses mirror this, facing ventrolaterally. The articular surfaces of both the pre- and postzygapophyses are almost flat and have subelliptical outlines. A short, deep, dorsoventrally oriented, and slit-like fossa separates the postzygapophyses medially in posterior view. The neural spines are transversely compressed subrectangular plates with subparallel anterior and posterior margins in lateral view and straight dorsal margins. The dorsal margins of the spines are slightly expanded mediolaterally relative to the spine bases, so that the top of spine forms a flat narrow platform.

With the exception of a few uninformative fragments, no dorsal ribs are preserved in any of the available specimens.

Sacral Vertebrae—The sacrum consists of six sacral vertebrae (IVPP V15939, Fig. 4; IVPP V12542, Fig. 5). Three anterior sacrals are preserved in articulation with the ilium and posterior dorsals in IVPP V15719 (Fig. 6). In all cases, with the exception of the last two sacral vertebrae in IVPP V15939 (which are slightly disarticulated), the sacral vertebrae are tightly connected, but are not co-ossified. IVPP V15939 is preserved with all six sacrals in articulation with the right ilium, via five pairs of sacral ribs (attaching to sacral vertebrae 2–6), and the first six caudal vertebrae. As the best-preserved specimen, IVPP V15939 forms the basis for most of the following description. All of the sutural contacts between the centra and sacral ribs, adjacent sacral ribs, and between the sacral ribs and ilia are unfused in this specimen. However, the neural arches are fused to the centra in sacrals 2–6, but the neurocentral suture is still visible in sacral 1.

Six sacral vertebrae occur in many basal ornithopods, including *Haya* (Makovicky et al., 2011), *Orodromeus* (Scheetz, 1999), *Parksosaurus*, *Thescelosaurus*, *Othnielosaurus* (Norman et al., 2004b), and some specimens of *Hypsilophodon* (NHMUK R193;

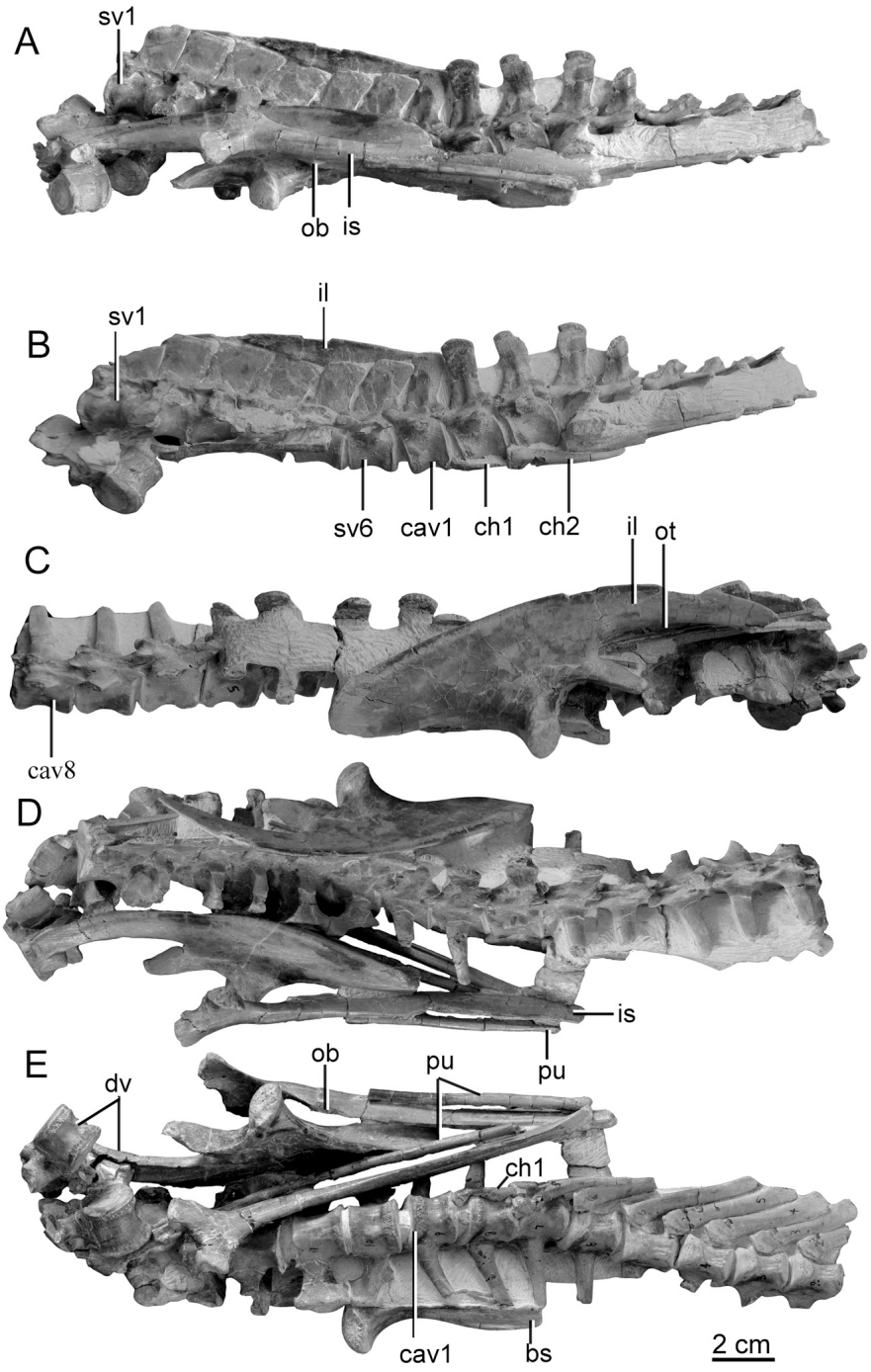

FIGURE 4. Posterior dorsal vertebrae, sacrum, anterior caudal vertebrae, and pelvic girdle elements of *Jeholosaurus shangyuanensis* (IVPP V15939). **A**, left lateral view; **B**, left lateral view with pubis and ischium removed; **C**, right lateral view; **D**, dorsal view; **E**, ventral view. **Abbreviations**: **bs**, brevis shelf; **cav**, caudal vertebrae; **ch**, chevron; **dv**, dorsal vertebrae; **il**, ilium; **is**, ischium; **ob**, obturator process; **ot**, ossified tendons; **pu**, pubis; **sar**, sacral rib; **sv**, sacral vertebrae.

Galton, 1974), as well as in the basal ceratopsian *Psittacosaurus* (You and Dodson, 2004) and heterodontosaurids such as *Heterodontosaurus* and *Fruitadens* (Butler et al., 2012). Five sacral vertebrae are present in more primitive ornithischians, including *Lesothosaurus* (Sereno, 1991), *Agilisaurus* (ZDM T6011; Peng, 1992), *Hexinlusaurus* (ZDM T6001; He and Cai, 1984; Barrett et al., 2005), and probably *Eocursor* (Butler et al., 2007). Sacra with more than six sacral vertebrae occur in derived ornithopods (Norman, 2004) and ceratopsians (Dodson et al., 2004).

In IVPP V15939, the anterior articular surface of sacral 1 is gently concave and transversely expanded in anterior view, so that the centrum is wider than high and subelliptical in outline. The posterior articular surface of sacral 1 is obscured by contact with sacral 2, but is clearly wider than the anterior articular surface. The dorsolateral portion of the centrum supports the anterior part of the second sacral rib. In lateral view, the surfaces of the centrum are strongly concave longitudinally and do not possess any nutrient foramina. Matrix obscures much of the ventral surface, which is separated from the lateral surfaces by distinct changes in slope. Due to breakage, the diapophyses are missing from sacral 1 in IVPP V15939. However, diapophyses are present in IVPP V15719, in which they are short, anterolaterally

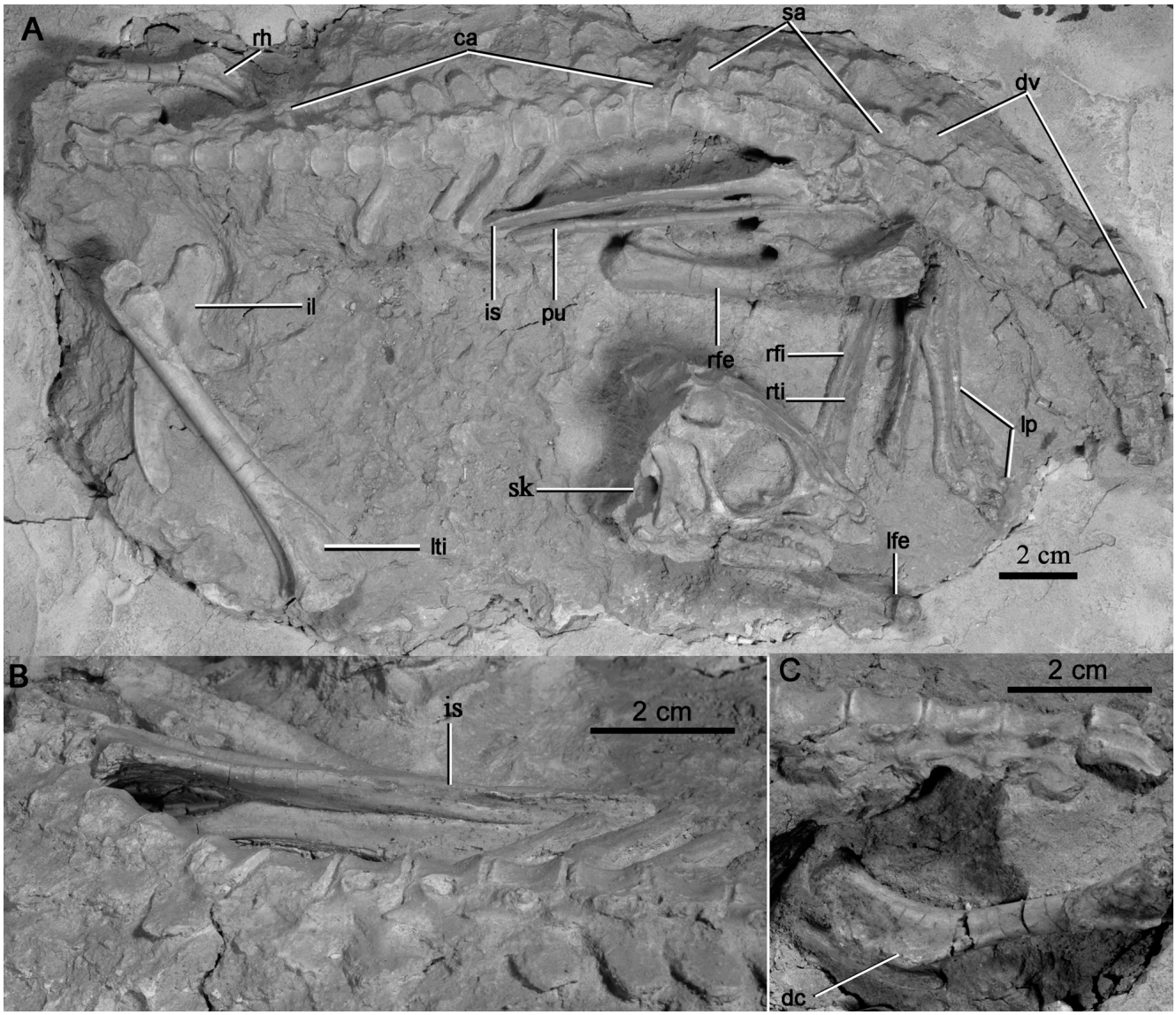

FIGURE 5. Postcranial skeleton of *Jeholosaurus shangyuanensis* (IVPP V12542). **A**, lateral view of the whole skeleton; **B**, ischia in posterior view; **C**, right humerus in anterior view. **Abbreviations**: **ca**, caudal vertebrae; **dc**, deltopectoral crest; **dv**, dorsal vertebrae; **il**, ilium; **is**, ischium; **lfe**, left femur; **lp**, left pes; **lti**, left tibia; **pu**, pubis; **rfe**, right femur; **rfi**, right fibula; **rh**, right humerus; **rti**, right tibia; **sa**, sacral vertebrae; **sk**, skull.

directed, and similar in morphology to those of the posterior dorsals. On this basis, it seems likely that sacral rib 1 was free and would not have been fused to the vertebra. In IVPP V15939, the prezygapophyses face dorsally and the neural spine is transversely compressed and plate-like with a subrectangular outline in lateral view. The posterior margin of the neural spine is closely appressed to that of sacral 2. Details of the postzygapophyses are not visible in IVPP V15939 due to the close apposition of sacral 2. In lateral view, small openings are present between each of the sacral vertebrae, positioned ventral to the articulated pre- and postzygapophyses and dorsal to the centrum. A thin platform of bone extends along the lateral surface of the neural arch, connecting the prezygapophysis to the diapophysis and diapophysis to the postzygapophysis, in a position equivalent to the prezygodiapophyseal and postzygopophyseal laminae of saurischian dinosaurs (Wilson, 1999). This platform is transversely narrow in dorsal view and continuous between the first four sacrals. It is still present on sacral 5, though not prominent as in sacrals 1–4 and is strongly reduced on sacral 6.

A large facet for the reception of the posterior part of the second sacral rib is present on the anterolateral surface of the centrum in sacral 2. The rest of the lateral surface is strongly concave anteroposteriorly and bears several small nutrient foramina. Low ridges separate the lateral and ventral surfaces of the centrum. The third sacral rib contacts the posterodorsal corner of the centrum, but there is no large facet for its reception. In ventral view, the anterior articular surface of sacral 2 is transversely expanded and subequal in width to the posterior articular surface of sacral 1, forming laterally projecting bosses for the articulation of the sacral rib. Posterior to this point the centrum narrows transversely and the width of the posterior articular surface is narrower than that of the anterior surface. The ventral surface of the centrum bears a broad, shallow, anteroposteriorly extending groove that is bounded laterally by the ridges that divide the ventral and lateral surfaces. Neural spine morphology is identical

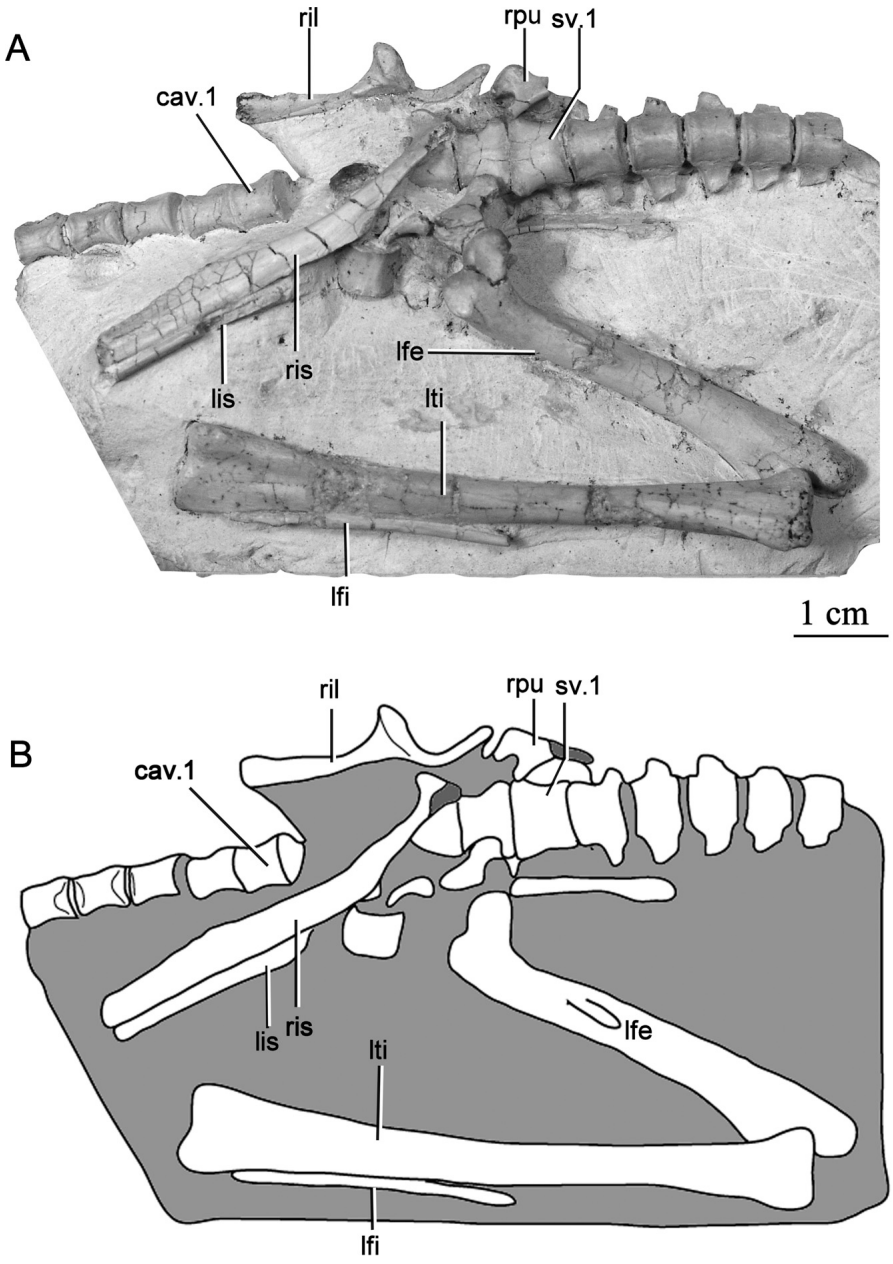

FIGURE 6. Pelvic region of *Jeholosaurus shangyuanensis* (IVPP V15719) in ventral view. **A**, photograph; **B**, outline drawing. **Abbreviations**: **cav.1**, caudal vertebra 1; **lfe**, left femur; **lfi**, left fibula; **lis**, left ischium; **lti**, left tibia; **ril**, right ilium; **ris**, right ischium; **rpu**, right pubis; **sv.1**, sacral vertebra 1.

to that of sacral 1 and the spines of sacrals 1 and 2 are the same dorsoventral height in lateral view, though the spine of sacral 2 is slightly longer than that of sacral 1. Unfortunately, the pre- and postzygapophyses are largely obscured by their close apposition to each other. The diapophyses extend laterally and ventrally as a thick bar that articulates with the sacral rib ventrally and they maintain a constant anteroposterior width in dorsal view. The anterior and posterior surfaces of the diapophyses are excavated, so that a deep fossa is formed on each surface, with that on the anterior surface extending onto the dorsal part of the sacral rib. The posterior fossa is deeper than the anterior fossa.

In ventral view, the anterior articular surface of sacral 3 is equal in width to the posterior margin of sacral 2. However, the centrum expands transversely towards its posterior surface. The anteroventral ridges dividing the ventral from the lateral surfaces of the centrum are more clearly defined than in sacral 2, and the ventral concavity on sacral 3 is correspondingly deeper. A single small nutrient foramen is present in the center of the lateral surface. The anterodorsolateral part of the centrum bears an elongate facet that extends for almost half of the length of the centrum, which accommodates most of the base of the third sacral rib. A smaller facet for articulation with the anterior part of the fourth sacral rib is present on the posterodorsolateral corner of the centrum. The neural arch of sacral 3 is effectively identical to that of sacral 2, although in dorsal view the diapophysis is slightly shorter in sacral 3.

In almost all respects, sacral 4 is very similar to sacral 3 and only differences are noted here. Sacral 4 has anterior and posterior articular surfaces that are subequal in width in ventral view, unlike in sacrals 1–3 in which one articular surface is more strongly expanded than the other. Sacral 4 also possesses the deepest ventral concavity of any sacral vertebra. The lateral

surface of the centrum possesses a single nutrient foramen, but this is displaced more ventrally and posteriorly than in the preceding sacrals because of the presence of a large attachment for sacral rib 4.

In ventral view, the centra of sacrals 5 and 6 are subequal in anterior and posterior widths. All of their articular surfaces are transversely narrower than the posterior articular surface of sacral 4. Sacrals 5 and 6 still possess the ventral concavity, but they are less clearly offset from the lateral surfaces than sacrals 2–4. Distinct ridges separating the lateral and ventral surfaces of the centrum are absent in sacral 5, but they are present in sacral 6 in which they are similar to those occurring in sacral 3. These ventral concavities are absent or poorly developed in IVPP V15719, a smaller individual, so it is possible that these features are subject to individual or ontogenetic variation. The posterior articular surface of sacral 6 is bordered by rugose ornament as also occurs in some dorsal vertebrae. Sacral 5 possesses one nutrient foramen on the lateral surface of the centrum and two foramina are present in the same position on sacral 6. Anterolaterodorsally, the centrum of sacral 5 bears a large facet for the fifth sacral rib that extends almost halfway along the centrum. There is no facet for sacral rib 6, which is borne completely on the centrum of sacral 6 and extends for almost two-thirds of centrum length. The diapophyses for sacrals 5 and 6 appear to be longer and more robust than those of the preceding sacrals, but this may, in part, be due to minor breakage of the latter. The distal ends of the diapophyses in these vertebrae are strongly expanded anteroposteriorly, so that they are 'T'-shaped in dorsal view. The neural arches and spines are very similar to those described for the preceding sacrals, although the neural spines are anteroposteriorly shorter in sacrals 5 and 6 than in sacral 4. In sacral 6, the neural spine, which is the tallest of the sacral neural spines, bears a ridge or swelling that arises on the posterior part of the lateral surface and that merges with the rest of the spine dorsally. This ridge forms the posterior margin of a shallow excavation that extends along the base of the spine.

In dorsal view, the diapophyses articulate with each other distally to form a narrow sacricostal yoke that encloses a series of large, subcircular sacral foramina (the margins of these foramina are complete between sacrals 2–3 and 5–6, whereas the other diapophyses are at least partially broken distally; Fig. 4D).

Caudal Vertebrae—The most complete caudal series is present in IVPP V12542, which has caudal vertebrae 1–15 preserved in articulation in right lateral view (Fig. 5). IVPP V15939 includes the first nine caudal vertebrae in articulated series (Fig. 4); five anterior caudals are preserved in articulation in IVPP V15719, in right lateral and ventral views (Fig. 6); and IVPP V12529 includes several articulated sections of the tail, consisting of middle and distal caudals (Fig. 7). In IVPP V12529, the neurocentral sutures of the middle caudals are unfused, whereas those of the distal caudals are fused. All of the neurocentral sutures in the anterior tail of IVPP V15939 are closed.

All of the caudal vertebrae are amphiplatyan or have gently concave articular surfaces. In IVPP V15939, the centrum of caudal 1 has an anterior articular surface that is as tall as it is wide, and the centrum length is also approximately equal to these two diameters (Fig. 4B). These proportions change gradually along the anterior portion of the tail, with anterior caudal centra further along the series becoming longer than they are tall and developing posterior articular surfaces taller than wide (Fig. 4C). Both the lateral and ventral surfaces of the centra are very gently concave anteroposteriorly and these surfaces are separated from each other by low, but distinct ridges. The lateral and ventral surfaces of caudals 1–6 bear some small, irregularly distributed nutrient foramina, but these appear to be absent thereafter. The ventral surface of the anterior caudals in IVPP V 15939 bears a shallow groove, which contains a faint midline ridge. However, these features are absent in IVPP V15719 and in this specimen the ventral and lateral surfaces are not separated by ridges, but grade into each other. These differences may be ontogenetic as IVPP V15719 is considerably smaller than IVPP V15939.

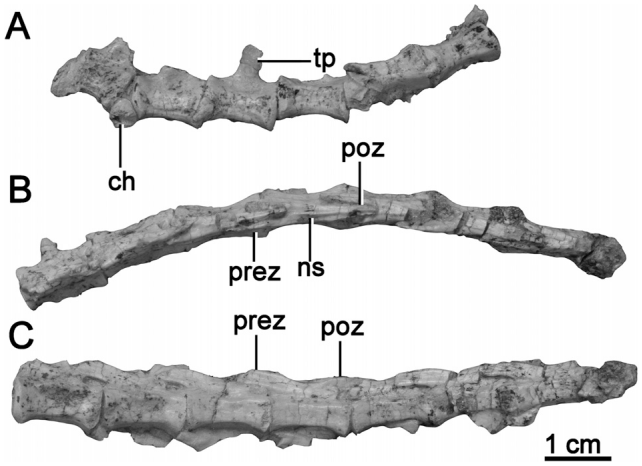

FIGURE 7. Caudal vertebrae of *Jeholosaurus shangyuanensis* (IVPP V12529). **A**, middle caudal vertebrae in lateral view; **B**, a series of posterior caudal vertebrae in dorsal view; **C**, posterior caudal vertebrae in lateral view. Exact positions of these sequences within the tail are unknown. **Abbreviations**: **ch**, chevron; **ns**, neural spine; **poz**, postzygapophysis; **prez**, prezygapophysis; **tp**, transverse process.

In IVPP V15939, posterior chevron facets are present from the second caudal onward and an anterior facet appears in caudal 3 and subsequent vertebrae. There is some variation in this character, however, as IVPP V12542 appears to lack chevrons on the first two vertebrae (Fig. 5A). In addition, although IVPP V15719 has posterior chevron facets on caudals 2 and 3, it does not gain anterior chevron facets until caudal 4. The chevron facets have a subcrescentic outline in anterior or posterior view and the posterior facets are more prominent than the anterior facets. The transverse processes of the anterior caudals (broken at their bases in all specimens except IVPP V15939) project horizontally, and curve slightly posteriorly in their distal part. They are elongate and taper distally to a rounded terminus.

Anterior caudal vertebrae have gracile neural spines, which are anteroposteriorly narrower and dorsoventrally taller than those of the sacral vertebrae, and which are inclined slightly posterodorsally. The spines of the first four caudals are approximately equal in height, but after this point they decrease in height caudally (Figs. 4, 5). In IVPP V15939, the neural spines of anterior caudals 1–5 have a teardrop-shaped transverse cross-section, with plate-like anterior margins and posterior margins that are slightly expanded transversely. This cross-section reflects expansion of the ventroposterolateral margin of the neural spine, which occurs in the same manner as in sacral vertebra 6 (see above). However, the development of this feature is more marked in the anterior caudals than in the posterior-most sacral, so that the shallow excavation bordered by this swelling on the lateral surface of the neural spine is more obvious than that seen in sacral 6. Breakage of the neural spines or poor preservation prevents determination of how far this feature continues along the proximal part of the tail. In IVPP V15939, the articular surfaces of the pre- and postzygapophyses are more steeply inclined than in either the dorsal or sacral vertebrae, being oriented at approximately 60° to the horizontal. The prezygapophyseal articular surfaces are larger and broader than those of the postzygapophyses.

Neither the pre- nor postzygapophyses extend far beyond the anterior or posterior margins of the centrum. In lateral view, the postzygapophyses are positioned dorsal to the level of the prezygapophyses.

The middle and posterior caudals of IVPP V12529 are poorly preserved and generally lack most of the neural arch (Fig. 7). The middle caudals are essentially smaller versions of the anterior caudals, although they exhibit a trend toward elongation of the centra, and still bear chevrons and short transverse processes. Some of the centra retain a faint ventral groove.

Posterior caudals become significantly more elongate, being at least twice as long as they are high and the centra have a subrectangular cross-section (Fig. 7). Ventral grooves are absent. Small transverse processes and chevron facets are present on the anterior-most posterior caudals, but are absent more distally. In the posterior caudals, the postzygapophyses fuse along the midline to form a single unified structure. Both the pre- and postzygapophyses become very elongate, extending well beyond the anterior and posterior limits of the centrum and exhibiting considerable overlap. The articular facets of the zygapophyses become almost vertically inclined.

Chevrons—Eight chevrons are preserved in articulation with the anterior-most caudal vertebrae of IVPP V15939 and can be seen in anterior, dorsal, and lateral views (e.g., Fig. 4B, E). Four chevrons are preserved in articulation with the anterior tail in IVPP V12542 (Fig. 5A), and IVPP V12529 includes three broken, disarticulated chevrons. The following description is based on IVPP V15939. In anterior or posterior view, the chevrons are approximately 'Y'-shaped with a transversely expanded proximal end consisting of two stout processes that merge distally to form the chevron blade. These processes form the lateral margins of the hemal canal, which is bridged dorsally by a continuous bar of bone that bears the articular facets for the caudal vertebrae. The chevron blade tapers distally, to form a transversely compressed sheet. In lateral view, the proximal end of the chevron is wedge-shaped and dived into anterodorsally and posterodorsally facing articular surfaces; the anterior articular surface is smaller than the posterior surface. The chevrons are anteroposteriorly expanded proximally, but narrow ventrally. In chevron 2, the shaft tapers in lateral view and its distal end curves slightly posteriorly, but in most other chevrons the anterior and posterior margins are subparallel and the distal margin is squared-off. Chevron 8 differs from this general pattern in having a distal end that is expanded anteroposteriorly relative to the shaft. Chevron 2 is longer than chevron one, and the anterior-most chevrons appear to show an increase in overall length, at least up to chevron 5 or 6, though many of the chevrons are broken distally preventing determination of their total length.

Ossified Tendons—Ossified tendons are found extending alongside the neural spines of the dorsal and sacral vertebrae in IVPP V15719, but are absent from the tail region. The tendons are long and slender and cylindrical in cross-section. In IVPP V15939, ossified tendons are preserved adjacent to the neural spines of the sacrum and might have extended on to the first or second caudal vertebra (Fig. 5C). This distribution of ossified tendons is similar to that in the early ornithischians *Lesothosaurus* (Thulborn, 1972), *Agilisaurus* (Peng, 1992), and *Heterodontosaurus* (Santa Luca, 1980), some ornithopods (e.g., *Haya*: Makovicky et al., 2011), and some basal ceratopsians and ceratopsids (Dodson et al., 2004). However, it differs from the condition seen in other ornithopods (e.g., *Hypsilophodon*: Galton, 1974) and some species of *Psittacosaurus* (e.g., *P. xinjiangensis*) in which ossified tendons extend along the caudal vertebrae. The tendons lack a distinct lattice-like arrangement and appear to be arranged in linear bundles. There is no evidence for the tendons extending onto anterior dorsals or cervical vertebrae in any specimen.

Pectoral Girdle and Forelimb

Scapula—A left scapula is preserved in IVPP V15719, but its posterior portion is partially damaged so the full extent of any posterior expansion cannot be assessed (Fig. 2A). The scapula and coracoid are unfused as also occurs in the majority of small ornithischians (e.g., Galton, 1974; Scheetz, 1999), with the exceptions of *Koreanosaurus* (Huh et al., 2010) and *Oryctodromeus* (Varricchio et al., 2007) in which a fused scapulocoracoid is present. The scapula shaft is slender and blade-like with a dorsoventrally convex lateral surface. The dorsal margin of the shaft is gently convex, whereas the ventral margin is concave. Towards its posterior end, the blade expands slightly dorsoventrally and it is bowed laterally along its entire length. Proximally the shaft expands dorsoventrally to form the proximal plate, which comprises the humeral glenoid and the articular surface for the coracoid (Fig. 2B). The dorsal margin of the proximal plate is damaged and incomplete, but forms a low ridge-like acromial process, whereas a second low ridge forms the ventral margin of the proximal plate, supporting the glenoid. These two ridges merge into the base of the scapula blade caudally. The proximal plate lacks the supraglenoid fossa and supraglenoid buttress present in *Yueosaurus* (Zheng et al., 2012). The dorsal part of the proximal plate anterior margin forms a subcrescentic articular surface for the coracoid. The ventral portion of the scapula anterior margin forms the glenoid cavity, which is slightly concave dorsoventrally, has a 'D'-shaped outline, and is transversely expanded relative to the rest of the proximal plate (Fig. 2B).

The scapula is very similar to that of other cerapodans and small ornithischians, including *Agilisaurus* (ZDM T6011; Peng, 1992), *Changchunsaurus* (Butler et al., 2011), *Haya* (Makovicky et al., 2011), *Hexinlusaurus* (ZDM T6001; He and Cai, 1984), *Hypsilophodon* (NHMUK R196; Galton, 1974), *Psittacosaurus* (Sereno, 1990), and *Yueosaurus* (Zheng et al., 2012), but it does not appear to be as elongate as that of *Heterodontosaurus* (SAM-PK-K1332; Santa Luca, 1980). In contrast to *Jeholosaurus*, *Koreanosaurus* possesses a scapula blade with a straight dorsal margin in lateral view (Huh et al., 2010) and both *Koreanosaurus* and *Oryctodromeus* possess strongly developed acromial ridges (Varricchio et al., 2007; Huh et al., 2010). Damage to the proximal and distal ends of the scapula prevent additional comparisons with these other taxa.

Coracoid—The left coracoid is preserved in IVPP V15719 in partial articulation with the scapula (Fig. 2B). In lateral view, it is a small subquadrate plate with a slightly convex external surface. A very small coracoid foramen appears to be present close to its posterior margin. All of the margins of the coracoid are broken, preventing meaningful comparisons with other taxa.

Humerus—A left and a right humerus are preserved in IVPP V15719 and IVPP V12542, respectively, both of which have suffered some damage to their proximal ends. In anterior view, the humerus of IVPP V15719 is elongate, slender, and approximately 70% the length of femur (Fig. 8). The proximal end is gently inclined medially, with the humeral head positioned at a level dorsal to the medial tubercle. This medial curvature is more strongly developed in the larger individual IVPP V12542 (Fig. 5C), which potentially indicates some ontogenetic variation in this character. The anterior surface of the proximal end is mediolaterally concave, with this concavity bounded laterally by the presence of the anteriorly extending deltopectoral crest, which is oriented at approximately 90° to the humeral shaft. The deltopectoral crest is complete in IVPP V12542 (Fig. 5C; present but damaged in IVPP V15719, see Fig. 8) and is triangular in outline. The medial margin of this proximal concavity is formed by a well-defined low ridge that is continuous with the medial tubercle. Ventral to point at which the deltopectoral crest merges with the shaft, the shaft is elliptical in cross-section. The distal end of the humerus is slightly expanded transversely with respect to the

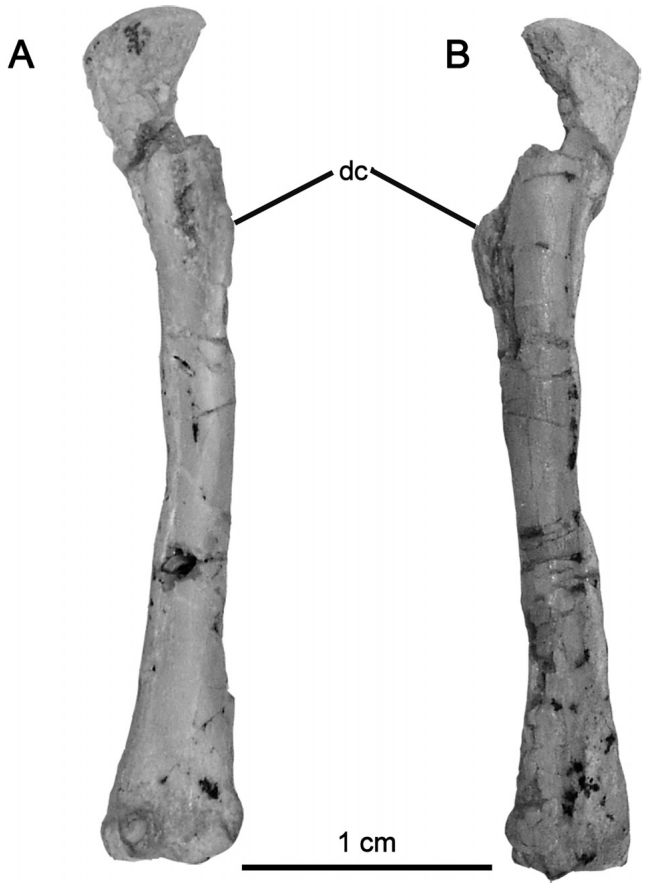

FIGURE 8. Left humerus of *Jeholosaurus shangyuanensis* (IVPP V15719). **A**, anterior view; **B**, posterior view. **Abbreviation**: **dc**, deltopectoral crest.

shaft, to form the two articular condyles, which are dumbbell-shaped in distal end view. The medial ulnar condyle is broader than the lateral radial condyle, and projects slightly further anteriorly. The anterior surface of the distal end bears a shallow, broad intercondylar fossa, whereas the posterior surface is flattened. In general, the morphology of humerus is exceptionally similar to that of *Changchunsaurus* (Butler et al., 2011), *Haya* (Makovicky et al., 2011), *Hypsilophodon* (NHMUK R196; Galton, 1974), *Orodromeus* (Scheetz, 1999), *Psittacosaurus* (Averianov et al., 2006), and *Yueosaurus* (Zheng et al., 2012), but it differs from the much stouter humeri present in *Koreanosaurus* and *Oryctodromeus*, in which the shafts are relatively shorter and wider relative to the total length of the bone (Varricchio et al., 2007; Huh et al., 2010).

Pelvic Girdle and Hind Limb

Ilium—Both ilia are present and well preserved in IVPP V15939: the left ilium is essentially fully visible, whereas the medial surface of the right ilium is largely obscured by matrix and its contact with the sacrum (Figs. 4, 9A, D). The left ilium (in lateral view) and right ilium (again, in lateral view only) are well preserved in IVPP V12542 (Fig. 5A) and IVPP V15719 (Fig. 6), respectively. Most of the following description is based on IVPP V15939, supplemented with observations from the other specimens.

The ilium is anteroposteriorly elongate, consisting of a gracile preacetabular process, a dorsoventrally tall main body, and a stout postacetabular process (Figs. 4C, 9A, D). In lateral view, the surface of the ilium is flat to slightly concave, and the dorsal margin of the ilium is convex in outline. Numerous short, fine, dorsoventrally oriented striations are present around its dorsal margin. In dorsal view, the ilium is bowed medially, due to slight lateral deflection of the preacetabular process (of approximately 10° from the midline; Fig. 4D).

The preacetabular process accounts for approximately 40% of total ilium length. In lateral view, the surface of the preacetabular process is gently concave dorsoventrally (Figs. 4C, 9A). The process tapers anteriorly, reducing in dorsoventral height, and curves anteroventrally. The medial surface of the process bears a prominent ridge, which extends posteroventrally from its origin at a point approximately halfway along the dorsal margin of the preacetabular process, fading into the main body of the ilium just dorsal to the ischial peduncle (Fig. 9D). This ridge forms the dorsal border of a deep elongate groove that tapers posteriorly and merges into the base of the pubic peduncle. The groove is defined ventrally by a sharp medially extending shelf, which gives the preacetabular process an almost 'L'-shaped transverse cross-section. This medial shelf has a flat ventral surface. In dorsal view, the narrow dorsal margin of the preacetabular process undergoes a slight decrease in its transverse width along its length.

The postacetabular process is shorter and deeper than the preacetabular process, and accounts for 36% of ilium length, similar to the condition in many basal ornithischians and ornithopods, including *Haya* (Makovicky et al., 2011), *Hexinlusaurus* (ZDM T6001; He and Cai, 1984), and *Hypsilophodon* (NHMUK R196; Galton, 1974). It differs from *Psittacosaurus* (Sereno, 1990) and *Yinlong* (IVPP V14530; F.-L.H., pers. observ.), which have pre- and postacetabular processes of almost equal length, from *Orodromeus*, in which the postacetabular process is relatively longer than the preacetabular process (Scheetz, 1999), and from *Heterodontosaurus*, whose postacetabular process accounts for only ~25% of total ilium length (SAM-PK-K1332; Santa Luca, 1980). The dorsal margin of the process begins as a narrow ridge anteriorly, but thickens posteriorly to terminate in an obliquely oriented truncated surface. The posteroventrolateral margin of the postacetabular process forms a prominent ridge that extends anteroventrally to merge with the ischial peduncle. This ridge forms the lateral margin of the brevis fossa. However, the brevis fossa is not visible in lateral view (Fig. 9A), a character that also occurs in many ornithopods (e.g., *Changchunsaurus* [Butler et al., 2011], *Hypsilophodon* [NHMUK R196; Galton, 1974], and *Orodromeus* [Scheetz, 1999]), in contrast to the condition in basal ornithischians such as *Agilisaurus* (ZDM T6011; Peng, 1992), *Scelidosaurus* (NHMUK R1111), *Stormbergia* (NHMUK R11000; Butler, 2005), and some basal ornithopods (e.g., *Haya* [Makovicky et al., 2011]) in which the brevis fossa is visible in lateral view. The brevis fossa is essentially absent in *Psittacosaurus* (Averianov et al., 2006), but is present in *Yinlong* (Xu et al., 2006). In ventral view, the brevis fossa is elongate, shallow, and transversely narrow. It is defined dorsally by a prominent brevis shelf that merges into the medial surface of the ischial peduncle cranially.

In lateral view, the acetabulum is fully open and is not backed by a sheet of bone medially (Figs. 4C, 9A). A very weak supraacetabular buttress is present as a low ridge forming the dorsal margin of the acetabulum, but this is not developed into a distinct flange. The pubic peduncle is triangular in outline and in transverse cross-section. It projects anteroventrally and slightly laterally, forming an angle of approximately 30° with the preacetabular process, and tapers distally. It is not as robust as, and is slightly shorter than, the ischial peduncle. The ischial peduncle is subtriangular in lateral view, with a subovate articular surface that is directed laterally and slightly anteroventrally. As in most basal ornithopods (e.g., *Haya* [Makovicky et al., 2011], *Hypsilophodon* [NHMUK R2477; Galton, 1974], and *Orodromeus*

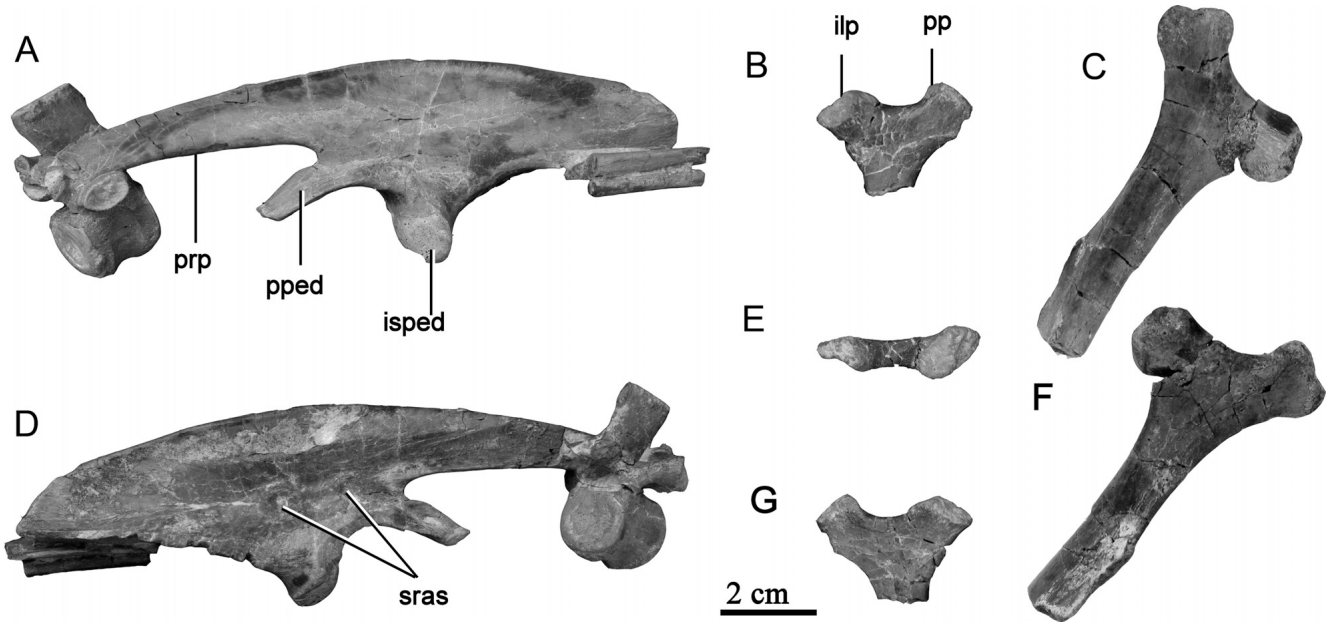

FIGURE 9. Pelvic girdle of *Jeholosaurus shangyuanensis* (IVPP V15939). **A**, left ilium in lateral view; **B**, right proximal ischium in lateral view; **C**, left proximal ischium in lateral view; **D**, left ilium in medial view; **E**, right ischium in dorsal view; **F**, left ischium in medial view; **G**, right ischium in medial view. The pelvic elements were detached from the main pelvic block of IVPP V15939 for photography. **Abbreviations**: **ilp**, iliac process; **isped**, ischiac peduncle; **pp**, pubic process; **pped**, pubic peduncle; **prp**, preacetabular process; **sras**, sacral rib attachment scar.

[Scheetz, 1999]), the ischial peduncle is more robust than the pubic peduncle.

The dorsal portion of the medial surface of the iliac main body is obscured in most specimens, but where visible is largely flat and featureless. The medial surface of the pubic peduncle is deeply excavated to form an attachment scar for sacral 1 and two prominent subelliptical scars on the medial surface of the main body represent the attachment sites for sacral ribs 2 and 3.

Ischium—Ischia are preserved in IVPP V12542 (right ischium only; Fig. 5A), IVPP V15719 (complete right ischium and broken, partially obscured left ischium; Fig. 6), and IVPP V15939 (both ischia present and complete, although both proximal ends can be separated from the block containing most of the pelvic material; Figs. 4A, D, E and 9B–C and E–G). The proximal end of the ischium consists of two processes that arise from a central plate: a posterodorsally facing iliac process and an anteriorly extending pubic process (Fig. 9B–C, E–G). The pubic process is a little longer than the iliac process and is also more compressed transversely. An angle of approximately 120° separates the processes in lateral view, and the region between them forms the ischiadic contribution to the acetabulum. The acetabular surface is smoothly convex anteroposteriorly and maintains an almost constant width along its entire length. The lateral surface of the pubic process is gently convex dorsoventrally and this convexity is maintained over most of the lateral surface of the proximal plate and becomes stronger as the proximal plate merges into the shaft. In contrast, the lateral surface of the iliac process is concave dorsoventrally. In anterior view, the pubic articulation has an inverted 'L'-shaped outline, due to the presence of a small, medially extending process from the dorsomedial corner of the otherwise subrectangular articular surface. A similarly shaped pubic articular surface also occurs in *Hypsilophodon* (Galton, 1974). The articular surface on the iliac process is divided into two facets: a dorsolaterally facing smooth area with a subovate outline, and a posteriorly facing rugose surface with a subtriangular outline. The medial surface of the proximal plate is generally concave anteroposteriorly, except for the iliac process, which is anteroposteriorly convex.

The posteroventral corner of the proximal plate gives rise to the shaft, which has an elliptical cross-section in its proximal part. The shaft undergoes torsion just distal to the proximal plate, so that the majority of the shaft lies in a plane set at approximately 120° to the anteroposterior plane of the proximal plate. In IVPP V15939, the dorsolateral surface of the proximal shaft bears a shallow, distinct groove, which originates just posterior to the junction between the plate and the shaft and that terminates at a point approximately level with the anterior margin of the obturator process. This groove was present along the lateral surface of shaft in IVPP V15939. However, this groove is absent in IVPP V12542 and IVPP V15719; the presence or absence of this feature might represent an ontogenetic or taphonomic variation. The ventromedial margin of the shaft possesses a proximally positioned prominent tab-like obturator process (Fig. 4A, D; which is usually broken distally), as in *Agilisaurus* (ZDM T6011; Barrett et al., 2005), *Haya* (Makovicky et al., 2011; although in this taxon the process is more distally positioned than in *Jeholosaurus*), *Hexinlusaurus* (ZDM T6001; He and Cai, 1984), *Orodromeus* (Scheetz, 1999), and *Stormbergia* (NHMUK R11000; Butler, 2005). This differs from the condition in *Hypsilophodon* (NHMUK R196; Galton, 1974) in which the obturator process is present but more distally positioned, and from *Eocursor* (Butler, 2010), *Lesothosaurus* (Butler, 2005), *Heterodontosaurus* (SAM-PK-K1332; Santa Luca, 1980), and basal ceratopsians (You and Dodson, 2004), which all lack the obturator process. Posteriorly the shaft becomes dorsoventrally flattened and transversely expanded, to produce a sheet-like cross-section. The lateral margin of the shaft thins to a greater extent than the medial margin, and forms a sharp edge. By contrast, the medial margin develops into a thickened ridge that runs along the dorsal margin of the distal-most third of the shaft. The medial surface of the distal shaft is concave. The ischiac shafts are appressed to each other for approximately 70% of their lengths distally.

Elongate ischiac symphyses also occur in basal ornithischians, including *Agilisaurus* (ZDM T6011; Barrett et al., 2005), *Eocursor* (Butler, 2010), and *Lesothosaurus* (NHMUK RUB17; Butler, 2005). In *Agilisaurus*, the symphysis accounts for approximately 50% of ischial length (Barrett et al., 2005). Elongate distal symphyses are absent in *Hypsilophodon* (Galton, 1974) and *Stormbergia* (Butler, 2005). The length of the ischiac symphysis cannot be measured accurately in *Haya* due to damage (see Makovicky et al., 2011), but the more distally positioned obturator process of this taxon indicates that its ischiadic symphysis must have been relatively shorter than that of *Jeholosaurus*.

Pubis—No complete pubis is preserved, but the morphology of the pubes can be nearly entirely reconstructed by combining information from IVPP V12542, IVPP V15719, and IVPP V15939 (Figs. 4–6). IVPP V12542 and IVPP V15939 both include a nearly complete right pubis, but the proximal plate is damaged in both specimens. IVPP V15939 also includes the pubic rod of the left pubis, whereas IVPP V15719 possesses a partial right pubis consisting of the proximal plate and a small section of the shaft.

In IVPP V15719 and IVPP V15939, the preserved part of the proximal pubis is a transversely compressed plate of bone. The lateral surface of this plate is shallowly concave in the former specimen and gently convex in the latter (Fig. 6). Most of the description of the proximal plate is based on IVPP V15719 because the prepubic process and iliac articular surface are broken in IVPP V15939. The posterodorsal margin of the proximal plate is slightly expanded transversely to form a subrectangular articular surface for the ilium. Anteriorly, the plate tapers to form a slender prepubic process with a cylindrical transverse cross-section, as also occurs in a number of basal ornithischians and basal ornithopods, including *Haya* (Makovicky et al., 2011), *Hexinlusaurus* (ZDM T6001; He and Cai, 1984), *Hypsilophodon* (NHMUK R195; Galton, 1974), and *Orodromeus* (Scheetz, 1999). However, none of the available specimens preserves a complete prepubic process, so it is not possible to determine if it terminated anterior or posterior to the anterior end of the iliac preacetabular process. The posteroventral part of the proximal plate expands mediolaterally to form the base of the pubic rod.

It cannot be established with certainty if the obturator notch was open or closed because the margins of this opening are partially broken in all specimens (Figs. 5, 6). However, in IVPP V15719 the section of pubic rod ventral to the area where a notch might have been positioned has surfaces composed of finished bone, lacking any trace of a broken surface that might indicate the presence of a bony sheet that would have extended dorsally to close the posterior margin of the notch; consequently, it seems likely that a notch was present and opened posteriorly. This suggestion is also supported by the preserved morphology of the proximal plate in IVPP V15939, in which the ventral corner of the proximal plate appears to form a distinct ventrally directed process, which is separated from the rest of the plate by a notch with smooth concave margins. Open obturator notches are present in the majority of primitive cerapodans, including basal ceratopsians such as *Archaeoceratops* (Dong and Azuma, 1997) and *Psittacosaurus* (Averianov et al., 2006), basal ornithopods such as *Haya* (Makovicky et al., 2011), and more-derived ornithopods (Norman, 2004; Norman et al., 2004b) and ceratopsians (You and Dodson, 2004). This differs from the condition in basal ornithischians, such as *Agilisaurus* (ZDM T6011; Barrett et al., 2005), *Hexinlusaurus* (ZDM T6001; He and Cai, 1984), some specimens referred to *Stormbergia* (Butler, 2005), and the basal ornithopod *Orodromeus* (Scheetz, 1999) in which the notch is closed to form a foramen. This character is polymorphic in *Hypsilophodon*, as different individuals of this taxon exhibit either a notch or a foramen (Galton, 1974).

The pubic rod is elongate, extends parallel to the ischial shaft, and has a cylindrical transverse cross-section (Figs. 4D, E, 5A). In IVPP V12542 and IVPP V15939, the ventral surface of the proximal part of the shaft bears a shallow groove, which attenuates distally and disappears at a point approximately 25% of the distance along the shaft length from the proximal plate.

Femur—Both femora are essentially complete and well preserved in IVPP V15939 (Fig. 10G–L) and IVPP V12542 (Fig. 5A), though those of the latter specimen remain embedded in a block. The holotype specimen (IVPP V12529) includes an almost complete left femur, which is missing only the femoral the head and the distal part of the fourth trochanter, and the poorly preserved distal end of the right femur (Fig. 10A–F). The left femur of IVPP V15719 is almost complete (Fig. 6), but its fourth trochanter is broken, whereas the right femur is represented by its distal part only.

The femur is long, slender, and bowed anteriorly in lateral view (Fig. 10A, I). The degree of bowing varies somewhat between specimens, with that of smaller individuals, such as the holotype, being more marked than in IVPP V15939. Proximally the femoral head expands medially and slightly dorsally to form a large, subspherical articular condyle. This is offset from the rest of the proximal end by a constricted, saddle-shaped neck (the fossa trochanteris), which is concave mediolaterally and convex anteroposteriorly (Fig. 10G, K). A fossa trochanteris is present in *Changchunsaurus* (Butler et al., 2011), *Hypsilophodon* (NHMUK R196; Galton, 1974), *Koreanosaurus* (Huh et al., 2010), and *Orodromeus* (Scheetz, 1999), but absent in some basal ornithischians (e.g., *Heterodontosaurus* [Santa Luca, 1980], *Fruitadens* [Butler et al., 2012], *Hexinlusaurus* [He and Cai, 1984], and *Lesothosaurus* [Thulborn, 1972]), and psittacosaurids (e.g., *Psittacosaurus sibiricus* [Averianov et al., 2006]). The posterior surface of the femoral head is excavated by a deep groove (Fig. 10G, J), also present in *Changchunsaurus* (Butler et al., 2011), *Hypsilophodon* (NHMUK R196; Galton, 1974), *Koreanosaurus* (Huh et al., 2010), and *Orodromeus* (Scheetz, 1999), which marks the insertion of the M. iliotrochantericus (Maidment and Barrett, 2011). The greater trochanter is expanded anteroposteriorly, and its dorsal margin is gently convex in the same direction. In lateral view, a dorsoventrally extending ridge is present on the lateral surface of the greater trochanter and proximal femoral shaft. It represents a ventral extension of the proximal cleft separating the greater and anterior trochanters and extends parallel to the anterior margin of the anterior trochanter (Fig. 10A, I). A similar ridge also occurs in other small ornithischians (e.g., *Changchunsaurus* [Butler et al., 2011], *Hypsilophodon* [Galton, 1974], and *Micropachycephalosaurus* [Butler and Zhao, 2009]). This ridge divides the lateral surface of the proximal femur into a narrow anterior region (effectively the base of the anterior trochanter) for the M. iliofemoralis, and a broader, posterior region for the insertion of the M. puboischiofemoralis internus (Maidment and Barrett, 2011). The latter surface is finely striated and textured and is subdivided into anterior and posterior portions by a low dorsoventrally extending ridge. The anterior trochanter is a finger-like process with a suboval cross-section. In lateral and anterior views, the tip of the anterior trochanter terminates ventral to the dorsal margin of the greater trochanter (Fig. 10A, I, L). It is separated from the greater trochanter by a short cleft, as also occurs in many other small ornithischians, such as *Hypsilophodon* (e.g., NHMUK R196; Galton, 1974), *Orodromeus* (Scheetz, 1999), *Psittacosaurus* (Sereno, 1990), and *Yinlong* (F.-L.H., pers. observ.). This differs slightly from the condition in some basal ornithischians, including *Eocursor* (Butler et al., 2007) and *Hexinlusaurus* (He and Cai, 1984), in which the cleft separating the anterior and greater trochanters is deeper, and from heterodontosaurids such as *Heterodotosaurus* and *Fruitadens* in which the trochanters are fused to one another (Butler et al., 2012).

A well-developed pendant fourth trochanter is present on the posteromedial edge of the femoral shaft, and is situated on the

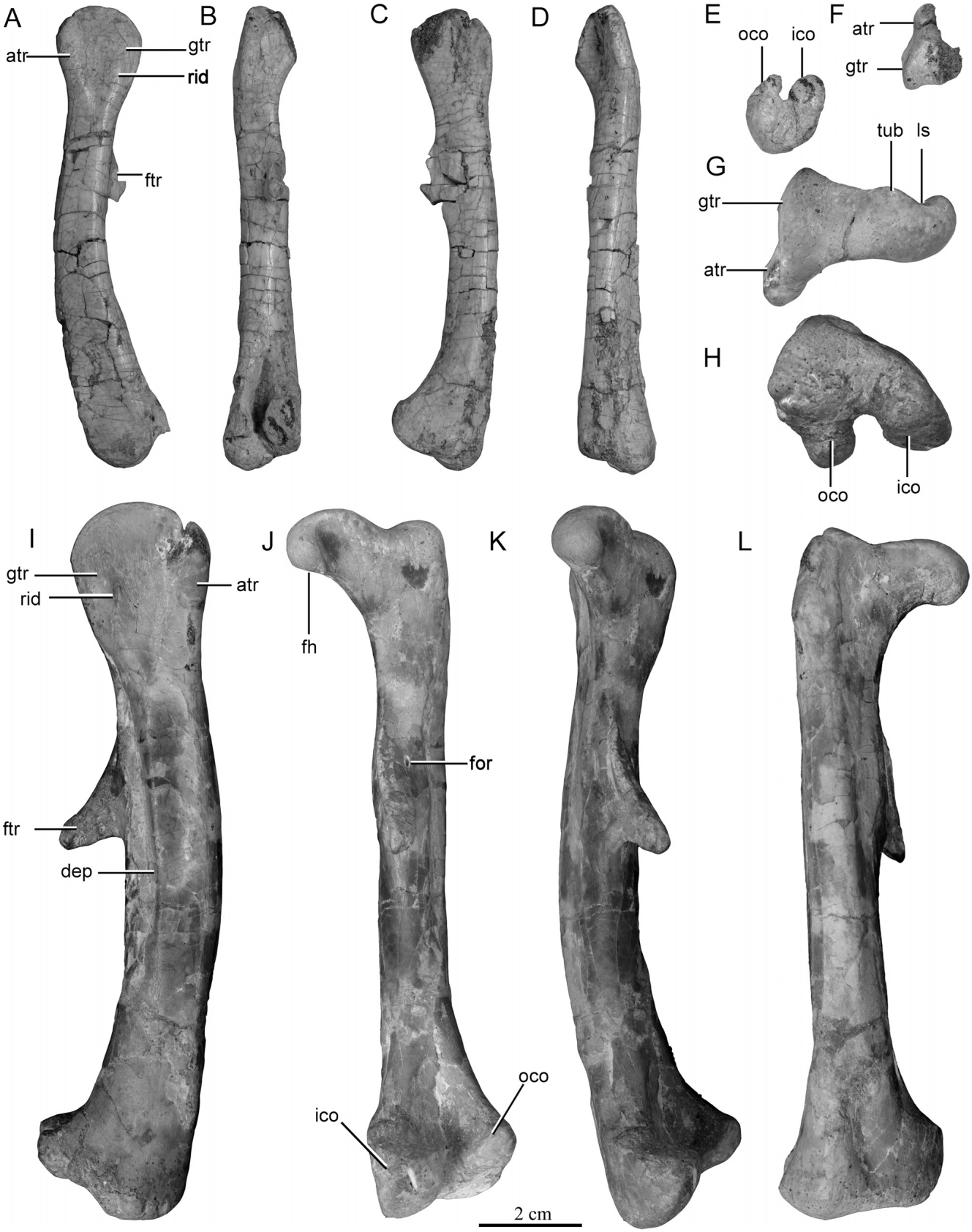

FIGURE 10. Femora of *Jeholosaurus shangyuanensis* (IVPP V12529 and IVPP V15939). Left femur of IVPP V12529 in **A**, lateral; **B**, posterior; **C**, medial; **D**, anterior; **E**, distal; and **F**, proximal views (note that the proximal head in missing in this specimen). Right femur of IVPP V15939 in **G**, proximal; **H**, distal; **I**, lateral; **J**, posterior; **K**, medial; and **L**, anterior views. **Abbreviations**: **atr**, anterior trochanter; **dep**, depression; **fh**, femoral head; **for**, foramen; **ftr**, fourth trochanter; **gtr**, greater trochanter; **ico**, inner condyle; **ls**, ligament sulcus; **oco**, outer condyle; **rid**, ridge; **tub**, tubercle.

proximal half of the shaft. In IVPP V12529, the distance from the ventral margin of the fourth trochanter to the proximal margin of the femur is approximately 45% of total femur length. The fourth trochanter has a flatted medial surface and it is convex laterally with a 'D'-shaped cross-section at its base, which becomes narrow and triangular distally. In IVPP V15939, a long, deep depression extends along the posterolateral margin of the shaft from a point just ventral to the greater trochanter, until a point approximately 75% of the distance from the proximal end. However, this feature is not present in any other specimen and is likely a result of crushing and deformation. A subcrescentic depression on the posteromedial margin of the shaft, adjacent to the fourth trochanter, is the insertion for the M. caudofemoralis brevis. A small circular foramen pierces the base of the fourth trochanter in posterior view, at a point approximately halfway along the contact between the process and the shaft in IVPP V12529 in IVPP V15939 (Fig. 10J). The shaft has a subcircular cross-section at midlength.

In IVPP V15939, the anterior surface of the shaft bears a shallow and wide depression, but this feature is absent or only incipiently developed in other individuals. An anterior intercondylar groove is absent. Xu et al. (2000) suggested that the absence of this feature might be diagnostic for *Jeholosaurus*, but many other small ornithopods and basal ornithischians also lack an intercondylar groove and this is an ornithischian symplesiomorphy (e.g., Norman et al., 2004b; Butler et al., 2008). All specimens exhibit a deep posterior intercondylar groove, separating the tibial and fibular epicondyles. In distal end view, the medial (tibial) condyle is transversely wider than the lateral (fibular) condyle and has a larger surface area (Fig. 10E, H). However, the two condyles extend for the same distance from the shaft posteriorly and also extend to the same point ventrally (except where deformation occurs, as in the left femur of IVPP V15939 and right femur of IVPP V12529). In distal view, the articular surface is quite rugose. A poorly developed shallow notch separates the lateral margin of the fibular condyle and the fibula epicondyle in distal view, as also occurs in *Hexinlusaurus* (He and Cai, 1984) and some individuals of *Hypsilophodon* (Galton, 1974).

Tibia—Both tibiae are present and complete in IVPP V12529, IVPP V12542, IVPP V15719, and IVPP V15939 (Figs. 5A, 6, 11). The tibiae are often preserved in articulation with the fibulae and the proximal tarsals. Tibiae of IVPP V15719 and IVPP V12542

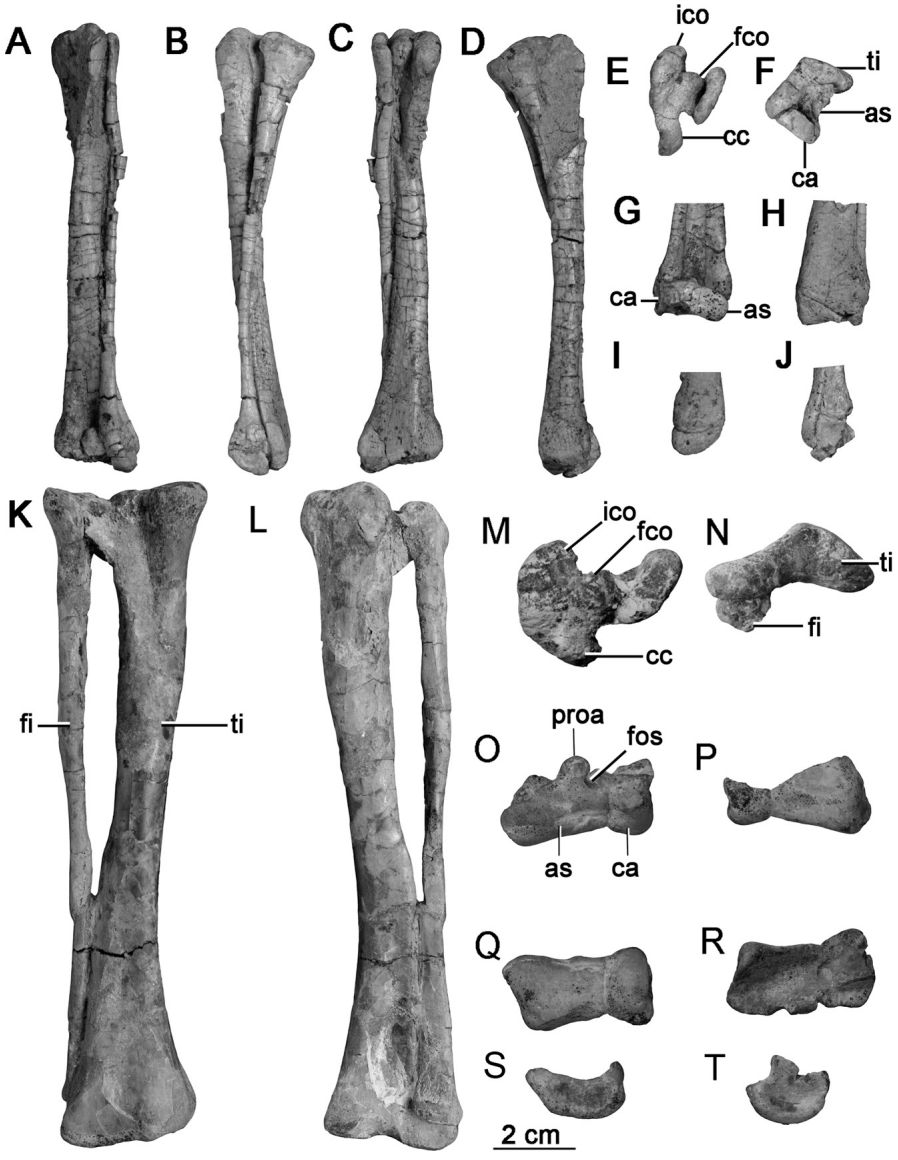

FIGURE 11. Left tibia, fibula, calcaneum, and astragalus of *Jeholosaurus shangyuanensis* (IVPP V15939 and IVPP V12529). Left tibia and fibula of IVPP V12529 in **A**, anterior; **B**, lateral; **C**, posterior; **D**, medial; **E**, proximal; and **F**, distal views. Distal part of right tibia and fibula, calcaneum, and astragalus of IVPP V12529 in **G**, anterior; **H**, posterior; **I**, medial; and **J**, lateral views. Left tibia and fibula of IVPP V15939 in **K**, posterior; **L**, anterior; **M**, proximal; and **N**, distal views. Left calcaneum and astragalus of IVPP V15939 in **O**, anterior; **P**, posterior; **Q**, ventral; and **R**, dorsal views; **S**, astragalus in medial view; **T**, calcaneum in lateral view. **Abbreviations**: **as**, astragalus; **ca**, calcaneum; **cc**, cnemial crest; **fco**, fibula condyle; **fi**, fibula; **fos**, fossa in 'forked' ascending process; **ico**, inner condyle; **proa**, ascending process of astragalus; **ti**, tibia.

are still partially embedded in matrix, whereas those of the other specimens have been completely prepared. The ratio of tibia to femur length ranges from 1.16 to 1.22 in IVPP V12529, IVPP V12542, and IVPP V15939, and is similar to that of *Hexinlusaurus* and *Hypsilophodon* (Barrett et al., 2005). However, this ratio is approximately 1.40 in the smallest specimen (IVPP V15719), which may represent individual or ontogenetic variation.

The tibia consists of proximal and distal expansions, linked by an elongate, slender shaft (Fig. 11). The proximal end consists of a robust, laterally compressed cnemial crest that extends anteriorly and slightly laterally, tapering toward a bluntly rounded apex. The cnemial crest is separated from the laterally extending fibula condyle by a deep narrow groove (Fig. 11E, M), in contrast to the much shallower groove separating these features in *Hypsilophodon* (Galton, 1974). A second well-defined sulcus separates the fibular condyle from the inner condyle posterolaterally (Fig. 11E, M). Taken together, the inner condyle and the cnemial crest give the proximal end a crescentic outline, with the fibula condyle extending from the center of the crescent's concave lateral surface. The cnemial crest, fibula condyle, and inner condyle have approximately equal dimensions in proximal view. The inner condyle tapers to the subtriangular, bluntly rounded apex, whereas the fibula condyle has a broader, subrectangular lateral margin. The latter bears a shallow notch, which is restricted to the surface of the condyle and does not extend further ventrally on to the surface of the shaft. The entire proximal articular surface is slightly rugose and anteroposteriorly convex.

Immediately ventral to the proximal expansion, the tibia narrows to form the shaft. The grooves originating from the sulci separating the inner condyle/fibula condyle and fibula condyle/cnemial crest extend along the posterolateral and anterolateral margins of the shaft, respectively. Both of these grooves attenuate ventrally and disappear at a point equal to approximately 25% of shaft length from the proximal end. The tibial shaft has a circular cross-section at midlength, but this becomes subtriangular towards the proximal and distal expansions. Distal to midlength, the anterolateral margin of the tibial shaft bears an elongate, low rounded eminence that articulates with the medial surface of the fibula. This eminence continues ventrally to merge with the lateral malleolus (Fig. 11A, C, K, L).

Distally, the shaft expands mediolaterally to form the malleoli, whose long axis is oriented transversely at approximately 90° to that of the proximal expansion. In anterior or posterior view, the lateral malleolus extends further ventrally and is mediolaterally wider than the medial malleolus (Fig. 11A, C, K, L). The anterior surface of the distal expansion bears a deep midline concavity whose ventral-most part would have accommodated the ascending process of the astragalus. In posterior view, the medial surface of the distal expansion is planar, the posterior surface is planar to very gently concave, and these surfaces are separated by a distinct break in slope, forming a low, proximally extending ridge that divides the medial and lateral malleoli. In distal end view, the articular surface is approximately 'L'-shaped, with the anterior surface of the anteroposteriorly narrow, transversely elongate, and laterally extending lateral malleolus forming an angle of around 120° with that of the anteroposteriorly expanded, transversely narrow, and posteromedially extending medial malleolus. The articular surfaces of both malleoli are rugose and end in blunt, rounded apices in distal end view.

In general, the tibiae of *Jeholosaurus* are very similar to those of *Changchunsaurus* (Butler et al., 2011), *Haya* (Makovicky et al., 2011), *Hypsilophodon* (NHMUK R5830; Galton, 1974), and *Orodromeus* (Scheetz, 1999), but are more gracile than those of *Psittacosaurus* (Averianov et al., 2006).

Fibula—Complete fibulae are present in all of those specimens that include tibiae; these two elements are usually preserved in articulation (Fig. 11). The fibula is an elongate slender element with small proximal and distal expansions. The proximal end is anteroposteriorly expanded with respect to the shaft, but is transversely compressed, producing a subelliptical outline in proximal view. The articular surface is gently convex anteroposteriorly and transversely. The medial margin of the proximal end is shallowly concave, and this area articulates with the fibula condyle of the tibia. This medial concavity continues onto the medial surface of the fibula shaft to create a shallow, ventrally extending groove that attenuates at a point approximately one-third of the way along the fibula. Ventral to this point, the fibula has a subcircular cross-section, which is maintained until a point just dorsal to the distal expansion, where the cross-section becomes subtriangular, with the apex of this triangle situated anteriorly. The minimum transverse width of the shaft in anterior view occurs at a point approximately two-thirds of the distance from the proximal end of the bone. The proximal half of the fibula shaft is separated from that of the tibia, whereas ventrally its medial margin is appressed to the tibia. The distal articular surface has a subtriangular outline in distal view, and is transversely expanded with respect to the shaft. The distal articular surface is convex and articulates with a facet on the calcaneum. The ventromedial corner of the fibula has a small contact with the astragalus. The fibula is not fused to the calcaneum (contra Zheng et al., 2012).

Astragalus—Both astragali are preserved in IVPP V15939 (Fig. 11O–R), an incomplete right astragalus and the ascending process of the left astragalus occurs in IVPP V12529 (adhered to the left tibia; Fig. 11G–H), and IVPP V15719 includes the right astragalus. The left astragalus is preserved in IVPP V12542, but the surface is obscured by matrix and it offers few useful details. In all specimens that preserve both elements, the astragalus and calcaneum are tightly appressed but do not fuse; the articulation between them remains at least partially open. The contact between the two elements occurs along a straight line that wraps around the anterior, ventral, and posterior surfaces, but cannot be traced dorsally.

In anterior view, the lateral margin of the astragalus contacts the calcaneum (Fig. 11O). Progressing medially, the dorsal margin gives rise to a short, spur-like ascending process, before extending ventrolaterally to form the rounded medial margin of the element. The medial margin of the astragalus is dorsoventrally shorter than its lateral margin. The anterior surface bears one or two small foramina, which are situated ventral to the ascending process; several areas of the surface are also slightly rugose, suggesting that they were areas of muscle attachment. The ascending process is subrectangular in anterior view, with a rounded dorsal margin, and extends dorsally and slightly laterally. A narrow, deep, mediodorsally extending fossa is present on the lateral side of the ascending process in both IVPP V12529 and IVPP V15939 (Fig. 11O). A similar feature, described as a 'forked ascending process,' is present in *Orodromeus* (Scheetz, 1999), but is absent in *Hypsilophodon* (Galton, 1974). A shallow depression extends mediolaterally across the anterior surface of the astragalus and on to the calcaneum; a similar depression is reported in *Haya* (Makovicky et al., 2011).

The astragalus has a crescentic outline in medial view (Fig. 11S). This medial surface is very gently concave, but becomes flatter as it tapers dorsally. In ventral view, the astragalus is anteroposteriorly widest medially and tapers laterally toward its contact with the calcaneum, giving it a wedge-like shape (Fig. 11Q). The ventral surface forms an anteroposteriorly convex articular region that blends smoothly into the posterior surface of the bone; the ventral and anterior surfaces are divided by an abrupt change of slope, although there is no distinct ridge.

In dorsal view, the proximal surface bears a series of complex articular facets for contacts with the tibia and fibula (Fig. 11R). A deep, obliquely oriented depression with a saddle-shaped articular surface would have received the lateral malleolus and the lateral-most portion of the medial malleolus. This facet consists of a deeply concave area laterally (the largest portion of the

facet) that is defined posteriorly by a prominent process arising from the posteromedial corner of the astragalus and delimited anteriorly by a low ridge that forms the dorsal margin of the anterior surface. Moving laterally, this facet arches dorsally to from a broad convex ridge that is defined posteriorly by the posteromedial process and anteriorly by the ascending process (Fig. 11R). A small dorsally facing facet with a subovate outline is situated immediately lateral to the base of the ascending process and forms a small surface for contact with the distal fibula. A small fossa is present on the dorsal surface close to the lateral margin of the element and may represent a remnant of the junction between the astragalus and calcaneum. In posterior view, the posteromedial process has a subtriangular outline that is tallest medially and reduces in height towards the calcaneum (Fig. 11H, P).

Calcaneum—Calcanea are present in all of the specimens that also possess the astragalus. The calcaneum is a small, block-like element whose lateral surface is hemispherical in outline and bears a concave surface that is surrounded by prominent ridge anteriorly and ventrally (Fig. 11T). A small triangular process extends posterodorsally from a point halfway along the element's posterodorsal margin and articulates with the distal end of fibula laterally (Fig. 11O–R). In dorsal view, this process marks the lateral end of a well-developed, mediolaterally extending ridge that divides the articular surface of the calcaneum into two facets: a small, shallow anterior part and a deeper, larger posterior part, which are separated from each other by an angle of approximately 130° (Fig. 11R). The anterior facet has a wedge-shaped outline and forms the articular surface for the distal fibula. It is confluent with a small fibula facet on the anterolateral corner of the astragalus (see above) and is bounded anteriorly by a low rim of bone that forms the anterodorsal margin of the calcaneum. The posterior facet is subrectangular in outline, continuous with the large tibial facet on the dorsal surface of the astragalus, and articulated with the lateral malleolus of the tibia. The latter facet is backed by a low ridge that forms the posterodorsal margin of the calcaneum. When in articulation, the posterior, posterodistal, and lateral surfaces of the tibia are still visible. In ventral view, the distal articular surface is strongly convex anteroposteriorly and bears a rounded lateral margin (Fig. 11Q). The ventral surface of the calcaneum reduces in anteroposterior width close to its junction with the astragalus, forming a narrow neck between the calcaneum and astragalus.

Distal Tarsals—Two distal tarsals (representing fused distal tarsals 1 and 2 and a separate distal tarsal 3) are preserved in articulation with the right pes of IVPP V15939 (Fig. 12G–K), with both feet of IVPP V12529 (though in the latter they are partially obscured by other elements; Fig. 12L–P), and the right pes of IVPP V15719 (Fig. 13). The distal tarsals are described with the foot held vertically.

Distal tarsals 1 and 2 appear to be fused to form a composite bone: there is no trace of a suture between them in either IVPP V12529 or IVPP V15939 (Fig. 12K, L). This does not appear to be under ontogenetic control given the size difference between these two specimens. In dorsal view, distal tarsal 1+2 is a squat, reversed 'L'-shaped element, with horizontal bar of the 'L' forming distal tarsal 1 (identified on the basis of it capping the proximal end of metatarsal 2), and the upright bar of the 'L' representing distal tarsal 2 (which caps the proximal end of a metatarsal 3). The element is dorsoventrally expanded along its lateral margin, but tapers medially, so that both the anterior and posterior surfaces are triangular in cross-section, with the tip of the triangle pointing dorsomedially in both cases. The anterolateral corner is the deepest part of the bone. The anterolateral surface bears a shallow crescentic concavity, whereas the rest of the proximal articular surface is almost flat. A shallow and broad sulcus extends dorsoventrally along the posterior surface of the bone and may represent a remnant of the junction between distal tarsals 1 and 2. The lateral surface is slightly concave anteroposteriorly in order to articulate with the medial margin of distal tarsal 3. In dorsal view, three shallow and narrow grooves are present on the posterior margin of distal tarsal 1+2 (Fig. 12G). Similar grooves are also present in the same position in some individuals in *Hypsilophodon* (NHMUK R200).

Distal tarsal 3 has a wedge-shaped outline with a convex lateral and slightly concave medial margin in proximal view (Figs. 12L, 13). The dorsal surface is concave and surrounded by a raised rim of bone, which would have articulated with the astragalus. In posterior view, a small foramen pieces on the center of the posterior surface. The anterior surface is slightly concave; the ventral and lateral surfaces are obscured by the presence of other elements. Distal tarsal 3 articulates with the proximal surface of metatarsal 4. In IVPP V15939, the proximal articular surface of metatarsal 4 is concave, suggesting that the ventral surface of distal tarsal 3 is convex.

Distal tarsal number is somewhat variable among ornithischians (e.g., Norman et al., 2004b). Two distal tarsals, sitting atop metatarsals 2–4, are present in *Agilisaurus* (Peng, 1992), *Hexinlusaurus* (He and Cai, 1984), *Lesothosaurus* (Thulborn, 1972), *Scelidosaurus* (Norman et al., 2004a), some pachycephalosaurs (Maryanska et al., 2004), basal ceratopsians (You and Dodson, 2004), and several basal ornithopods (Norman et al., 2004b; including *Haya* [Makovicky et al., 2011]). Three distinct, unfused distal tarsals are present in *Heterodontosaurus*, with distal tarsal 1 situated above metatarsals 1 and 2, distal tarsal 2 above metatarsals 3 and 4, and distal tarsal 3 above metatarsal 4 (Santa Luca, 1980). The condition in *Jeholosaurus* in which three distal tarsals are present, but with fusion of distal tarsals 1 and 2 (on the basis of positional relationships), is unusual, but a similar condition also appears to be present in *Orodromeus*. The latter taxon possesses a large "medial distal tarsal" (Scheetz, 1999:figs. 30D–F, 31), which is 'L'-shaped in proximal view, bears possible evidence of a line of fusion between potentially separate two ossification centers (a prominent ridge on its ventral surface; Scheetz, 1999:fig. 30E), and articulates with the proximal ends of metatarsals 2 and 3. Thus, this element may also represent the fused distal tarsals 1 and 2. An additional "lateral distal tarsal" (Scheetz, 1999:fig. 30G–I) could therefore be interpreted as a distal tarsal 3. This combination of features has not been described in any other ornithischians.

Metatarsus—Metatarsals are preserved in IVPP V12529, IVPP V15719, and IVPP V15939 (Figs. 12, 13). IVPP V15939 processes both articulated metatarsalia, including metatarsals 1–4 in each case (Fig. 12A, B), and in IVPP V15719 articulated metatarsals 1–4 are preserved on the right (Fig. 13) and metatarsals 2–4 on the left, with metatarsal 2 broken distally. In IVPP V12529, metatarsals 1–5 are preserved in the right pes but are generally damaged or obscured proximally, and metatarsals 1–4 are preserved in left pes (Fig. 12C–F). IVPP V12542 includes left metatarsals 2–4. All of the metatarsals lie in almost the same plane in IVPP V15719, IVPP V15939, and IVPP V12542, forming a posteriorly concave shallow arch in dorsal view (Figs. 12A, B, 13). By contrast, in IVPP V12529 the metatarsi have a more tubular arrangement, which was originally proposed as a diagnostic feature of *Jeholosaurus* (Xu et al., 2000; Fig. 12C–F). However, this tubular arrangement is due to transverse compression of the pedes, which has caused bunching of the metatarsals, and this morphology cannot be regarded as a useful diagnostic character. Metatarsal 3 is the longest and stoutest, with metatarsal 1 being approximately 50% of the length of metatarsal 3, as is common in basal ornithopods (Norman et al., 2004b). Metatarsals 2 and 4 are approximately equal in length (Figs. 12A, B, 13). The dorsal surface of the articulated metatarsus is transversely convex. Proximally, the metatarsals are expanded anteroposteriorly, especially in metatarsals 2 and 3. All of the metatarsal shafts are closely appressed throughout most of their lengths, separating

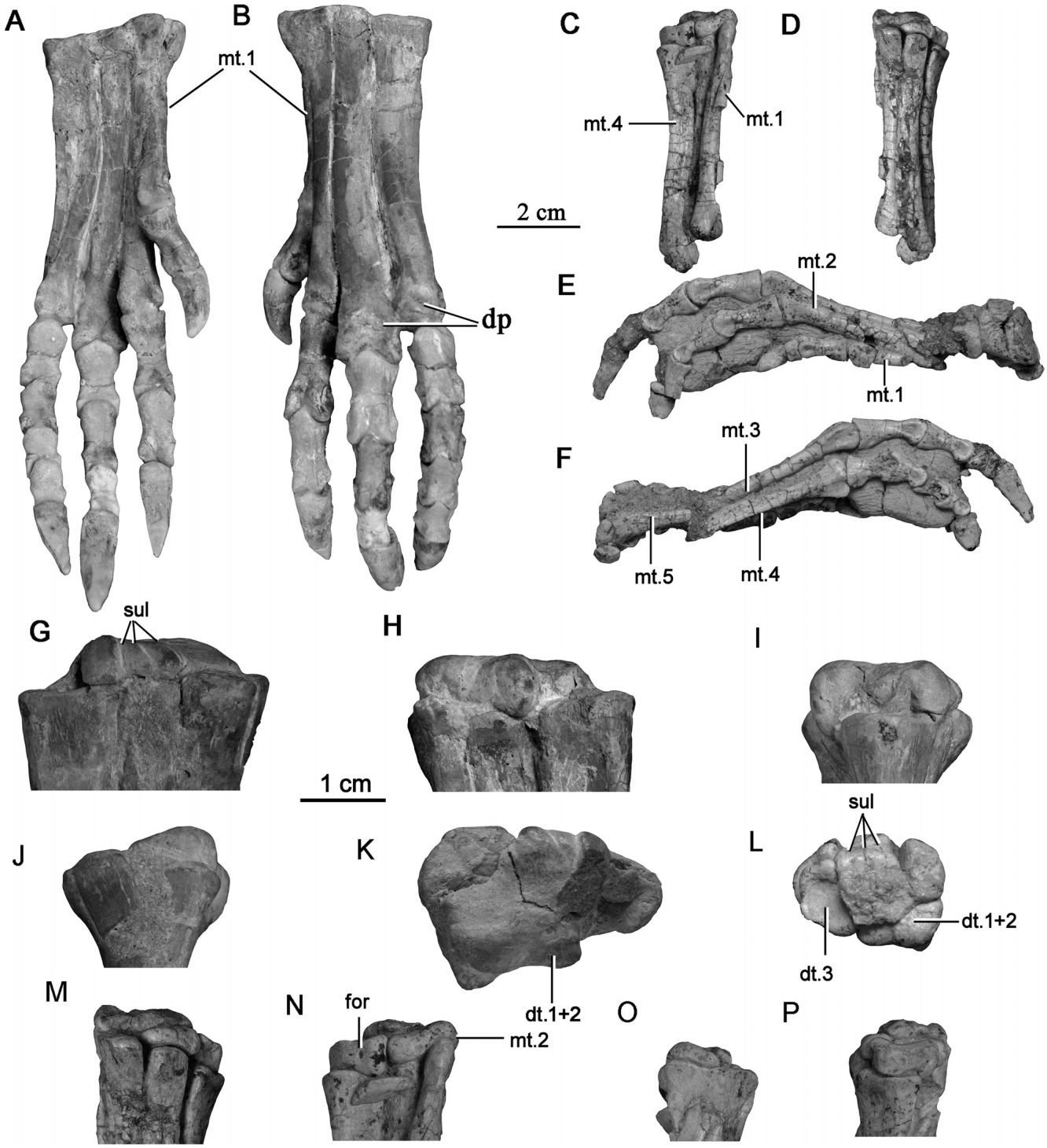

FIGURE 12. Pedes of *Jeholosaurus shangyuanensis* (IVPP V15939 and IVPP V12529). Left pes of IVPP V15939 in **A**, posterior/ventral and **B**, anterior/dorsal views (following the different orientations used to described the metatarsi and phalanges in the text). Left metatarsus of IVPP V12529 in **C**, posterior and **D**, anterior views. Right pes of IVPP V12529 in **E**, medial and **F**, lateral views. Distal tarsals of IVPP V15939 in **G**, anterior; **H**, posterior; **I**, medial; **J**, lateral; and **K**, proximal views. Distal tarsals of IVPP V12529 in **L**, proximal; **M**, anterior; **N**, posterior; **O**, lateral; and **P**, medial views. **Abbreviations**: **for**, foramen; **mt**, metatarsals; **dp**, dorsal pit; **dt.1+2**, fused distal tarsals 1 and 2; **dt.3**, distal tarsal 3; **sul**, sulci.

from each other ventrally just proximal to their distal articular surfaces. Many features of the metatarsals are obscured by the close apposition of these elements in the articulated feet of the available specimens. The metatarsi are described as held in a vertical orientation.

Metatarsal 1 is thin and splint-like proximally and does not articulate with the distal tarsals. Its proximal end terminates slightly ventral to the proximal end of metatarsal 2 and the shaft of metatarsal 1 is closely appressed to that of metatarsal 2 along its entire length. In medial view, it tapers ventrally, but expands

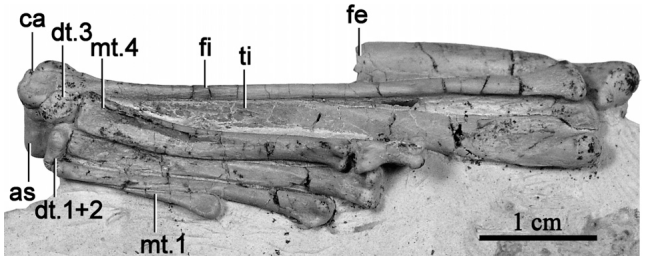

FIGURE 13. Right hind limb (in anterior view) and pes (in ventral view) of *Jeholosaurus shangyuanensis* (IVPP V15719). **Abbreviations**: **as**, astragalus, **ca**, calcaneum, **dt.1+2**, fused distal tarsals 1 and 2; **dt.3**, distal tarsal 3; **fe**, femur; **fi**, fibula, **mt**, metatarsals, **ti**, tibia.

anteroposteriorly towards its distal end to form the articular region for phalanx 1-1. As a result, the anterior margin of the shaft is strongly concave in medial view. In anterior view, the shaft of metatarsal 1 is mediolaterally compressed proximally and expands transversely distally. The distal end is weakly divided into lateral and medial condyles, which extend for the same distance ventrally in anterior view. A shallow ligament pit appears to be present on the medial side of this articular condyle (e.g., in the right metatarsal 1 of IVPP V15939), but there is no trace of a lateral ligament pit.

Metatarsal 2 has a subelliptical outline in dorsal view, with its long axis extending anteroposteriorly. The medial margin of the proximal end is slightly emarginated and forms the dorsal margin of shallow sulcus that extends a short distance along its medial margin to house the head of metatarsal 1. The shaft retains a subelliptical cross-section along its entire length, except in the distal articular region where it is subrectangular. In medial view, the shaft of the metatarsal constricts anteroposteriorly just ventral to the proximal end, forming a concave proximal anterior margin, which then expands at the distal end to form the articular surface for phalanx 2-1. The distal articular surface is more strongly expanded than the proximal end of the metatarsal, both transversely and anteroposteriorly. The shaft is essentially straight in both anterior and medial views and its lateral surface is closely appressed to metatarsal 3; however, in anterior view, the distal-most part of the shaft diverges a little medially, so that a short, narrow gap is present between it and the distal end of metatarsal 3. The distal end bears a subdivided articular condyle, with the medial condyle deflected medioventrally and slightly smaller than the lateral one. A distinct groove separates the medial and lateral condyles posteriorly, but does not extend on to the anterior surface of the shaft. A shallow pit is present on the medial surface of the shaft and a deeper, larger pit is on the lateral surface.

Metatarsal 3 has a subrectangular proximal surface that is weakly concave both medially and laterally for the reception of metatarsals 2 and 4. In anterior view, the shaft is straight in its proximal part, but curves laterally towards its distal end. The posterior surface bears a very shallow excavation, bounded medially and laterally by the margins of the shaft, which extends for approximately 80% of shaft length before fading out dorsal to the distal articular surface. As in metatarsal 2, the distal articular expansion is subrectangular in cross-section, with the articular surface divided into two condyles by a groove posteriorly. A shallow ligament pit is present on the medial surface of the distal articular expansion and a deeper pit occurs on the lateral surface. A deep fossa is formed on the anterior surface of the distal end, just dorsal to the articular surface.

Metatarsal 4 has a wedge-shaped outline in proximal view, with the narrow end of the wedge extending laterally. The shaft narrows in anteroposterior thickness ventrally and maintains a subtriangular cross-section, with the apex of the triangle extending laterally. However, the shaft expands anteriorly in its distal-most part to form a cylindrical cross-section, and then becomes subrectangular near to the distal end. In anterior view, the shaft of metatarsal 4 is deflected more laterally than that of the other metatarsals and has a sinuous outline. It extends parallel to metatarsal 3 in its proximal half, but diverges laterally from metatarsal 3 for much of the rest of its length. However, the distal-most end of the shaft changes course to extend more medially, bringing the distal end back into contact with metatarsal 3. In posterior view, the shaft is widest proximally, narrows distally, and expands slightly into the distal end. In distal view, the triangular cross-section of the shaft results in an anteroposteriorly expanded medial condyle and a reduced, ridge-like lateral condyle. In posterior view, a prominent longitudinal ridge arises from the medial margin of the shaft at a point approximately one-third of the way from the proximal end, and extends ventrally and progressively more laterally until it terminates close the lateral border of the shaft, and merges into the distal end.

Metatarsal 5 is present in the right pes of IVPP V12529 only. It is a small, slender, distally tapering, and splint-like element with a mediolaterally compressed proximal end. It is similar to those present in *Haya* (Makovicky et al., 2011), *Hypsilophodon* (Galton, 1974), and *Orodromeus* (Scheetz, 1999); it is not clear if metatarsal 5 was present or absent in *Changchunsaurus* (Butler et al., 2011).

Phalanges—Complete sets of phalanges are present in both feet of IVPP V12529 (Fig. 12E, F) and IVPP V15939 (Fig. 12A, B); IVPP V15719 includes phalanges 2-1 and 2-2 in the left pes and 4-1 in the right pes; and IVPP V12542 has phalanges 2-2 and 3-3 in right pes. In the following description, the phalanges are described as though held in plantigrade stance. The phalangeal count is 2-3-4-5-0, as occurs in a variety of other basal ornithopods, basal ceratopsians, and basal ornithischians (e.g., *Agilisaurus* [Peng, 1992], *Haya* [Makovicky et al., 2011], *Heterodontosaurus* [Santa Luca, 1980], *Hexinlusaurus* [He and Cai, 1984], *Hypsilophodon* [Galton, 1974], *Psittacosaurus* [Averianov et al., 2006], and probably *Changchunsaurus* [Butler et al., 2011]). Some of the phalanges are partially reconstructed or may have been added from other individuals.

In dorsal view, all of the non-ungual phalanges are essentially similar in morphology, differing only in proportions and subtle variations in the development of features, including the dorsal lappets and collateral ligament pits (see below; Fig. 12B). They consist of a constricted central shaft with concave margins that connects the transversely expanded proximal and distal articular surfaces. Well-developed, 'V'-shaped lappets extend posteriorly from the dorsal margins of all non-ungual phalanges, with the exception of phalanges 1-1, 2-1, 3-1, and 4-1 in IVPP V12529 and IVPP V15719, as also occurs in *Haya* (Makovicky et al., 2011) and *Hypsilophodon* (Galton, 1974). This difference may be due to either ontogeny, because IVPP V15939 is the largest individual, or some error in the reconstruction of the pes in the latter individual. In lateral view, the ventral margins of the shafts are curved and dorsally concave, whereas dorsal margins are straight and slopes ventrally. Both the proximal and distal articular surfaces are dorsoventrally expanded and this expansion is greater at the proximal end of the element. Both lateral and medial surfaces of the distal articular surfaces bear well-developed collateral ligament pits, and these become deeper and more clearly defined in distal phalanges. In anterior view, the distal end of each phalanx is divided into lateral and medial ginglymi, which bear a saddle-shaped articular surface.

All ungual phalanges are claw-like (Fig. 12A, B, E, F). In dorsal view, the unguals are broadest proximally, taper distally to a narrow tip, and lack dorsal lappets. Laterally, the proximal end is dorsoventrally expanded and the dorsal and ventral margins

of the ungual converge distally. The dorsal margin is arched and convex, whereas the ventral margin is deeply concave, producing a strongly curved, ventrally extending, sharp distal tip to the ungual. An elongate, shallow ligament groove originates from the proximal end of the ungual and extends for almost the full length of the element on both lateral and medial surfaces.

Phalanx 1-1 of *Jeholosaurus* is relatively short and does not extend to a point level with the distal end of metatarsal 2 (Fig. 12A); this contrasts with *Changchunsaurus*, which has a much more elongate phalanx 1-1 (Butler et al., 2011). The ungual phalanx of digit 3 is longer than the other unguals (Fig. 12A), as also occurs in *Hexinlusaurus* (He and Cai, 1984). This differs from *Changchunsaurus*, in which the length of the digit 2 ungual exceeds that of the digit 3 ungual (Butler et al., 2011). In addition, in *Jeholosaurus*, phalanx 3-4 is the longest in digit 3 (IVPP V12529: Xu et al., 2000), as also occurs in *Xiaosaurus* (Dong and Tang, 1983), whereas in *Agilisaurus* (Peng, 1992), *Changchunsaurus* (Butler et al., 2011), *Heterodontosaurus* (Santa Luca, 1980), *Hexinlusaurus* (He and Cai, 1984), *Hypsilophodon* (Galton, 1974), *Lesothosaurus* (Thulborn, 1972), and *Orodromeus* (Scheetz, 1999) this is not the case (Butler et al., 2011).

PHYLOGENETIC ANALYSIS

To reassess the phylogenetic position of *Jeholosaurus* based upon the new postcranial information provided here, we modified the matrix of Butler et al. (2011), correcting their scores for *Jeholosaurus* (see Appendix 2 for character scores and Supplementary Information for character list and data matrix; Supplementary Information available online at www.tandfonline.com/UJVP). In addition, we added four other East Asian small ornithischian taxa: the Early Cretaceous basal cerapodan *Albalophosaurus* (using character scores taken primarily from Ohashi and Barrett, 2009), the 'middle' Cretaceous *Yueosaurus* (scored based upon Zheng et al., 2012), the Late Cretaceous *Koreanosaurus* (scored based upon Huh et al., 2010), and the Late Cretaceous *Haya* (using character scores taken from Makovicky et al., 2011). Following Makovicky et al. (2011), *Bugenasaura* was deleted and their character scores were used for *Thescelosaurus*. The resultant data matrix consists of 227 characters and 54 taxa (see Supplementary Information; note that an all-zero 'dummy' character was added at the beginning of the matrix to aid with interpretation because TNT numbers characters beginning with '0'). Following Butler et al. (2011), five characters (112, 135, 137, 138, 174) were treated as ordered.

The matrix was analyzed using TNT (Goloboff et al., 2008). First, we analyzed the matrix under the 'new technology search' option, using sectorial search, ratchet, tree drift, and tree fuse options with default parameters and 100 random addition sequences. Second, these generated trees were analyzed under traditional TBR branch swapping (which more fully explores each tree island). The analysis recovered 3240 most parsimonious trees (MPTs) of 577 steps. Standard bootstrapping (sampling with replacement) was carried out using 1000 replicates and a new technology search (ratchet, with 10 random addition sequences). Reduced bootstrap standard frequencies were calculated excluding five wildcard taxa (see below).

The strict consensus of these trees does not recover a monophyletic Ornithopoda, and the phylogenetic positions of *Jeholosaurus*, *Changchunsaurus*, *Haya*, and the other East Asian taxa (with the exception of *Albalophosaurus*, which is resolved within Ceratopsia) are poorly resolved. The 50% majority-rule consensus tree places all of the East Asian taxa (again, with the exception of *Albalophosaurus*) within an unresolved polytomy at the base of Cerapoda. However, reduced consensus analysis (carried out using the 'Comparisons—Pruned Trees' option of TNT) demonstrated that *Yandusaurus hongheensis*, *Anabisetia*, *Echinodon*, *Yueosaurus*, and *Koreanosaurus* act as highly unstable 'wildcard' taxa. A strict reduced consensus tree calculated a posteriori excluding these taxa (Fig. 14) shows considerably greater resolution, and places *Jeholosaurus*, *Changchunsaurus*, and *Haya* together within a clade (Jeholosauridae), with *Jeholosaurus* and *Changchunsaurus* as sister taxa. Interestingly, *Koreanosaurus* is placed within Jeholosauridae in a 50% majority-rule reduced consensus tree when *Yandusaurus hongheensis*, *Anabisetia*, *Echinodon*, and *Yueosaurus* are excluded a posteriori, and *Yueosaurus*, which has not formerly been included within a cladistic analysis, is placed within Jeholosauridae in a 50% majority-rule reduced consensus tree when *Yandusaurus hongheensis*, *Anabisetia*, *Echinodon*, and *Koreanosaurus* are excluded a posteriori. Thus, these two East Asian taxa might prove eventually to be members of Jeholosauridae, but more detailed phylogenetic studies and new specimens of both are required to confirm this hypothesis. Jeholosauridae is consistently positioned basally within Ornithopoda in reduced consensus trees, but more derived than an *Orodromeus* + *Zephyrosaurus* clade. This result is consistent with that recovered by Makovicky et al. (2011).

It has also been suggested that *Koreanosaurus* forms a clade with the North American taxon *Orodromeus*, possibly together with *Oryctodromeus* and *Zephyrosaurus* (Huh et al., 2010). However, although *Orodromeus* and *Zephyrosaurus* are recovered as sister taxa by our analysis, we find no support for this more inclusive clade. Nevertheless, we cannot test this alternative hypothesis fully herein, because our data matrix excludes *Oryctodromeus*: only a brief description of this taxon has been published to date (Varricchio et al., 2007), which is inadequate to allow comprehensive character scoring, and we have not yet had the opportunity to examine this material ourselves.

DISCUSSION AND CONCLUSIONS

Although initially described as a basal ornithopod, Xu et al. (2000) noted that *Jeholosaurus* shared some characteristics with marginocephalians and retained a number of ornithischian symplesiomorphies. However, this work did not explore or discuss ornithischian interrelationships within a rigorous phylogenetic framework. Subsequently, incorporation of *Jeholosaurus* into a large-scale ornithischian phylogeny confirmed the suggestion of Xu et al. (2000), recovering *Jeholosaurus* as a basal member of Ornithopoda (Butler et al., 2008). This conclusion has been reinforced by the addition to this data set of new cranial data for this taxon (Barrett and Han, 2009) and, especially, cranial and postcranial data from *Changchunsaurus* and *Haya* (Butler et al., 2011; Makovicky et al., 2011). The new information on the postcranial anatomy of *Jeholosaurus* presented herein provides additional support for this conclusion and for the suggestion that these three taxa form a clade (Butler et al., 2011; Makovicky et al., 2011) that might have been endemic to East Asia during the Cretaceous. Although *Changchunsaurus*, *Haya*, and *Jeholosaurus* are very similar in overall anatomy, they can be distinguished by sets of cranial and postcranial autapomorphies, as well as unique combinations of character states (see comparative comments in Description, above), and probably represent a genuine radiation of small-bodied taxa. In this context, it is noteworthy that Xu et al. (2000) proposed that several Chinese genera spanning the Middle Jurassic–Early Cretaceous (*Agilisaurus*, *Hexinlusaurus*, *Jeholosaurus*, and *Xiaosaurus*) might have formed an endemic clade. However, three of these are currently thought to represent more basally positioned ornithischian taxa that lie outside of Ornithopoda (Butler et al., 2008). It is plausible that *Koreanosaurus* and *Yueosaurus* might also be closely related to, or included within, Jeholosauridae. Small ornithopods are generally rare in Eastern Asia and future work needs to resolve further the phylogenetic affinities of taxa including "*Gongbusaurus*" *wucaiwanensis* and *Yandusaurus hongheensis* in order to determine if

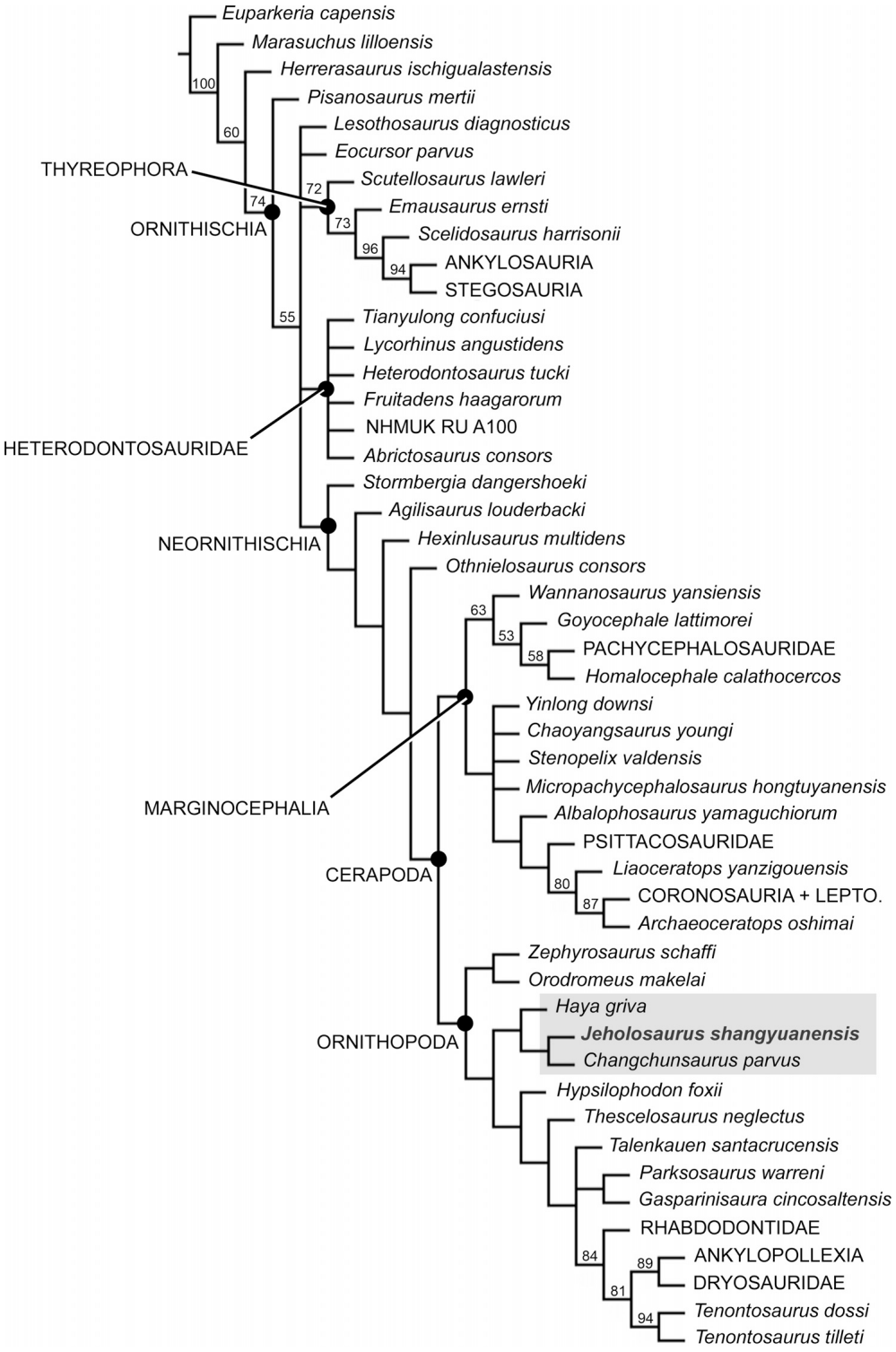

FIGURE 14. Strict reduced consensus tree of ornithischian interrelationships based on an analysis of 227 characters for 54 taxa (see text and Online Supplementary Information for details). Bootstrap values are shown above branches.

any other Chinese taxa might shed light on the early evolution of Jeholosauridae, or if they belong to other ornithischian lineages.

Although our analysis places *Jeholosaurus* within Ornithopoda, it should be noted that relationships among basal cerapodan taxa remain weakly supported, and it is possible that the addition of new taxa or characters will have a major influence on tree topology, especially because some basal ornithopods and basal marginocephalians are now known to be more similar to each other than acknowledged previously. This point is illustrated by a novel result from our analysis, which recovers the Early Cretaceous Japanese genus *Albalophosaurus* as a basal marginocephalian, contrary to the earlier analysis of Ohashi and

Barrett (2009) that could only resolve this taxon as a basal cerapodan.

ACKNOWLEDGMENTS

P.M.B. and R.J.B. would like to thank F.-L.H. and X.X. for their invitation to work on this material. Funding for P.M.B. to travel to China was provided by the Palaeontological Investment Fund of the NHMUK, and this project was carried out under the auspices of a Memorandum of Understanding between IVPP and NHMUK. Two anonymous referees provided useful comments on an earlier version of this paper. F.-L.H. and X.X. were supported by grants from the National Natural Science Foundation of China. R.J.B. is supported by the DFG Emmy Noether Programme (BU 2587/3-1).

LITERATURE CITED

Averianov, A. O., A. V. Voronkevich, S. V. Leshchinskiy, and A. V. Fayngertz. 2006. A ceratopsian dinosaur *Psittacosaurus sibiricus* from the Early Cretaceous of West Siberia, Russia and its phylogenetic relationships. Journal of Systematic Palaeontology 4:359–395.

Barrett, P. M., and F.-L. Han. 2009. Cranial anatomy of *Jeholosaurus shangyuanensis* (Dinosauria: Ornithischia) from the Early Cretaceous of China. Zootaxa 2072:31–55.

Barrett, P. M., R. J. Butler, and F. Knoll. 2005. Small-bodied ornithischian dinosaurs from the Middle Jurassic of Sichuan, China. Journal of Vertebrate Paleontology 25:824–834.

Beneden, P.-J. van. 1881. Sur l'arc pelvien chez les dinosauriens de Bernissart. Bulletins de l'Académie Royale des Sciences, des Lettres et des Beaux-Arts de Belgique, 3 série 1:600–608.

Butler, R. J. 2005. The 'fabrosaurid' ornithischian dinosaurs of the Upper Elliot Formation (Lower Jurassic) of South Africa and Lesotho. Zoological Journal of the Linnean Society 145:175–218.

Butler, R. J. 2010. The anatomy of the basal ornithischian dinosaur *Eocursor parvus* from the lower Elliot Formation (Late Triassic) of South Africa. Zoological Journal of the Linnean Society 160:648–684.

Butler, R. J., and Q. Zhao. 2009. The small-bodied ornithischian dinosaurs *Micropachycephalosaurus hongtuyanensis* and *Wannanosaurus yansiensi*s from the Late Cretaceous of China. Cretaceous Research 30:63–77.

Butler, R. J., R. M. H. Smith, and D. B. Norman. 2007. A primitive ornithischian dinosaur from the Late Triassic of South Africa, and the early evolution and diversification of Ornithischia. Proceedings of the Royal Society B: Biological Sciences 274:2041–2046.

Butler, R. J., P. Upchurch, and D. B. Norman. 2008. The phylogeny of the ornithischian dinosaurs. Journal of Systematic Palaeontology 6:1–40.

Butler, R. J., L.-Y. Jin, J. Chen, and P. Godefroit. 2011. The postcranial osteology and phylogenetic position of the small ornithischian dinosaur *Changchunsaurus parvus* from the Quantou Formation (Cretaceous: Aptian–Cenomanian) of Jilin Province, north-eastern China. Palaeontology 5:667–683.

Butler, R. J., L. B. Porro, P. M. Galton, and L. M. Chiappe. 2012. Anatomy and cranial functional morphology of the small-bodied dinosaur *Fruitadens haagarorum* from the Upper Jurassic of the USA. PLoS ONE 7:e31556.

Colbert, E. H. 1981. A primitive ornithischian dinosaur from the Kayenta Formation of Arizona. Museum of Northern Arizona Bulletin 53:1–61.

Dodson, P., C. A. Forster, and S. D. Sampson. 2004. Ceratopsidae; pp. 494–513 in D. B. Weishampel, P. Dodson, and H. Osmólska (eds.), The Dinosauria, Second Edition. University of California Press, Berkeley, California.

Dong, Z.-M., and Y. Azuma. 1997. On a primitive neoceratopsian from the Early Cretaceous of China; pp. 68–89 in Z. M. Dong (ed.), Sino-Japanese Silk Road Dinosaur Expedition. China Ocean Press, Beijing.

Dong, Z.-M., and Z.-L. Tang. 1983. Note on the new mid-Jurassic ornithopod from Sichuan Basin, China. Vertebrata PalAsiatica 21:168–172. [Chinese with English summary]

Galton, P. M. 1974. The ornithischian dinosaur *Hypsilophodon* from the Wealden of the Isle of Wight. Bulletin of the British Museum (Natural History), Geology 25:1–152.

Gilmore, C. W. 1913. A new dinosaur from the Lance Formation of Wyoming. Smithsonian Miscellaneous Contributions 61:1–5.

Gilmore, C. W. 1931. A new species of tröodont dinosaur from the Lance Formation of Wyoming. Proceedings of the United States National Museum 79:1–6.

Goloboff, P., F. C. Farris, and K. C. Nixon. 2008. TNT, a free program for phylogenetic analysis. Cladistics 24:774–786.

Granger, W., and W. K. Gregory. 1923. *Protoceratops andrewsi*, a preceratopsian dinosaur from Mongolia. American Museum Novitates 72:1–9.

Han, F.-L. 2009. Anatomy of Jeholosaurus shangyuanensis and phylogenetic analysis of basal Ornithischia. Unpublished M.Sc. thesis, Graduate School of Chinese Academy of Sciences Beijing, 133 pp.

He, H.-Y., X.-L. Wang, Z.-H. Zhou, F. Jin, F. Wang, L.-K. Yang, X. Ding. A. Boven, and R.-X. Zhu. 2006. $^{40}Ar/^{39}Ar$ dating of Lujiatun Bed (Jehol Group) in Liaoning, northeastern China. Geophysical Research Letters 33:L04393. .

He, X.-L., and K.-J. Cai. 1984. The Middle Jurassic Dinosaurian Fauna from Dashanpu, Zigong, Sichuan. Volume 1. The Ornithopod Dinosaurs. Sichuan Scientific and Technological Publishing House, Chengdu, 71 pp. [Chinese, with English summary]

Huh, M., D.-G. Lee, J.-K. Kim, J.-D. Lee, and P. Godefroit. 2010. A new basal ornithopod dinosaur from the Upper Cretaceous of South Korea. Neues Jahrbuch für Geologie und Paläontologie, Abhandlungen 259:1–24.

Huxley, T. H. 1869. On *Hypsilophodon*, a new genus of Dinosauria. Abstracts of the Proceedings of the Geological Society of London 204:3.

Maidment, S. C. R., and P. M. Barrett. 2011. The locomotor musculature of basal ornithischian dinosaurs. Journal of Vertebrate Paleontology 31:1265–1291.

Makovicky, P. J., B. M. Kilbourne, R. W. Sadleir, and M. A. Norell. 2011. A new basal ornithopod (Dinosauria, Ornithischia) from the Late Cretaceous of Mongolia. Journal of Vertebrate Paleontology 31:626–640.

Marsh, O. C. 1881. Principal characters of the American Jurassic dinosaurs. Part V. American Journal of Science (Series 3) 21:417–423.

Maryanska, T., R. E. Chapman, and D. B. Weishampel. 2004. Pachycephalosauria; pp. 464–477 in D. B. Weishampel, P. Dodson, and H. Osmólska (eds.), The Dinosauria, Second Edition. University of California Press, Berkeley, California.

Norman, D. B. 2004. Basal Iguanodontia; pp. 413–437 in D. B. Weishampel, P. Dodson, and H. Osmólska (eds.), The Dinosauria, Second Edition. University of California Press, Berkeley, California.

Norman, D. B., L. M. Witmer, and D. B. Weishampel. 2004a. Basal Thyreophora; pp. 335–342 in D. B. Weishampel, P. Dodson, and H. Osmólska (eds.), The Dinosauria, Second Edition. University of California Press, Berkeley, California.

Norman, D. B., H.-D. Sues, L. M. Witmer, and R. A. Coria. 2004b. Basal Ornithopoda; pp. 393–412 in D. B. Weishampel, P. Dodson, and H. Osmólska (eds.), The Dinosauria, Second Edition. University of California Press, Berkeley, California.

Ohashi, T., and P. M. Barrett. 2009. A new ornithischian dinosaur from the Lower Cretaceous Kuwajima Formation of Japan. Journal of Vertebrate Paleontology 29:748–757.

Owen, R. 1842. Report on British fossil reptiles. Part II. Reports of the British Association for the Advancement of Science 11:60–204.

Owen, R. 1863. Monograph on the British fossil Reptilia from the Oolitic Formations. Part Two. *Scelidosaurus harrisonii*. Palaeontographical Society Monographs 14(Number 60):1–26 + pls. 1–11.

Peng, G.-Z. 1992. Jurassic ornithopod *Agilisaurus louderbacki* (Ornithopoda: Fabrosauridae) from Zigong, Sichuan, China. Vertebrata PalAsiatica 30:39–51. [Chinese with English summary]

Russell, D. A., and X.-J. Zhao. 1996. New psittacosaur occurrences in Inner Mongolia. Canadian Journal of Earth Sciences 33:637–648.

Santa Luca, A. P. 1980. The postcranial skeleton of *Heterodontosaurus tucki* (Reptilia, Ornithischia) from the Stormberg of South Africa. Annals of the South African Museum 79:159–211.

Scheetz, R. D. 1999. Osteology of Orodromeus makelai and the phylogeny of basal ornithopod dinosaurs. Ph.D. dissertation, Montana State University, Bozeman, Montana, 186 pp.

Seeley, H. G. 1887. On the classification of the fossil animals commonly called Dinosauria. Proceedings of the Royal Society of London 43:165–171.
Sereno, P. C. 1986. Phylogeny of the bird-hipped dinosaurs (Order Ornithischia). National Geographic Research 2:234–256.
Sereno, P. C. 1990. Psittacosauridae; pp. 579–592 in D. B. Weishampel, P. Dodson, and H. Osmólska (eds.), The Dinosauria, first edition. University of California Press, Berkeley, California.
Sereno, P. C. 1991. *Lesothosaurus*, "fabrosaurids," and the early evolution of Ornithischia. Journal of Vertebrate Paleontology 11:168–197.
Thulborn, R. A. 1972. The postcranial skeleton of the Triassic ornithischian dinosaur *Fabrosaurus australis*. Palaeontology 15: 29–60.
Varricchio, D. J., A. J. Martin, and Y. Katsura. 2007. First trace and body fossil evidence of a burrowing, denning dinosaur. Proceedings of the Royal Society B: Biological Sciences 274:1361–1368.
Vickaryous, M. K., T. Maryanska, and D. B. Weishampel. 2004. Ankylosauria; pp. 363–392 in D. B. Weishampel, P. Dodson, and H. Osmólska (eds.), The Dinosauria, Second Edition. University of California Press, Berkeley, California.
Wang, X.-L., Y.-Q. Wang, Y. Wang, X. Xu, Z.-L. Tang, F.-C. Zhang, and Y.-M. Hu. 1998. Stratigraphic sequence and vertebrate-bearing beds of the lower part of the Yixian Formation in Sihetun and neighboring area, western Liaoning, China. Vertebrata PalAsiatica 36:81–101. [Chinese, with English summary]
Wilson, J. A. 1999. A nomenclature for vertebral laminae in sauropods and other saurischian dinosaurs. Journal of Vertebrate Paleontology 19:639–653.
Xu, X., X.-L. Wang, and H.-L. You. 2000. A primitive ornithopod from the Early Cretaceous Yixian Formation of Liaoning. Vertebrata PalAsiatica 38:318–325.
You, H.-L., and P. Dodson. 2004. Basal Ceratopsia; pp. 478–493 in D. B. Weishampel, P. Dodson, and H. Osmólska (eds.), The Dinosauria, Second Edition. University of California Press, Berkeley, California.
Zan, S.-Q., J. Chen, L.-Y. Jin, and T. Li. 2005. A primitive ornithopod from the Early Cretaceous Quantou Formation of central Jilin, China. Vertebrata PalAsiatica 43:182–193. [Chinese, with English summary]
Zheng, W.-J., X.-S. Jin, M. Shibata, Y. Azuma, and F.-M. Yu. 2012. A new ornithischian dinosaur from the Cretaceous Liangtoutang Formation of Tiantai, Zhejiang Province, China. Cretaceous Research 34:208–219.
Zhou, S.-W. 1984. The Middle Jurassic Dinosaurian Fauna from Dashanpu, Zigong, Sichuan. Volume 2. Stegosaurs. Sichuan Scientific and Technological Publishing House, Chengdu, 52 pp. + 13 pls. [Chinese, with English summary]

Submitted March 12, 2011; revisions received April 2, 2012; accepted April 25, 2012.
Handling editor: You Hailu.

APPENDIX 1. Measurements for girdle and limb elements (all given in mm) (Tables A1–A5). Measurements in plain type represent those take from complete elements; those in bold figures indicate minimum measurements taken from partially broken or damaged specimens; bold figures in parentheses are estimated total measurements from partially broken or damaged specimens. **Abbreviations**: **AP**, the direction in which a specimen was measured anteroposteriorly; **Dm**, the minimum height measured from the dorsal edge of the ilium to the dorsal margin of the acetabulum; **DV**, the direction in which a specimen was measured dorsoventrally; **L**, left; **Le**, the greatest length; **Lp**, the length from the proximal end of the pubic process of the ischium to the point at which the two ischial shafts meet along the midline; **Lpf**, the distance from the proximal end of the femur to the base of the fourth trochanter; **ML** indicate the direction in which a specimen was measured mediolaterally; **Mw**, the minimum width of the shaft; **R**, right; **Wd**, the greatest length of distal end; **Wp**, the greatest length of proximal end; **Wpp**, the mediolateral width of the pubic peduncle of the ilium.

TABLE A1. Measurements of the bones of the pectoral girdles.

Bone	Specimen number	L/R	Le (AP)	Le (DV)	Wp (DV)	Wp (AP)	Wd (DV)	Wd (AP)	Wd (ML)	Mw
Scapula	V15719	L	**27.2**	**—**	?	—	**7.8** (**9**)	—	—	5.3 (**DV**)
Coracoid	V15719	L	**—**	**8.9**	—	**10.4**	—	**10**	**—**	**8.2** (**AP**)
Humerus	V12542	R	**—**	61.5	**—**	15.8	**—**	**—**	**9.4** (**11.5**)	4.3 (**ML**)
Humerus	V15719	L	**—**	33.6	**—**	**5.1** (**5.5**)	**—**	**—**	6	2.4 (**ML**)

TABLE A2. Measurements of the ilium.

Bone	Specimen number	L/R	Le (AP)	Preacetabular process		Wpp	Dm
				Le (AP)	Width (DV)		
Ilium	V15939	L	**124**	**43.7**	15.2	11.5	27.5
	V15939	R	126.1	49.8	16.4	**11.1**	25.7
	V12542	L	77.4	26.8	10.0	—	—
	V15719	R	**39.7** (**41.0**)	13.6	5.2	2.4	8.4

TABLE A3. Measurements of the ischium and pubis.

Bone	Specimen number	L/R	Length	Wp (AP)	Wd (AP)	Mw	Lp
Ischium	V15939	L	133.8	30.1	13.6	4.3	37.7
	V15939	R	137.4	31.5	11.4	4.3	—
	V12542	L	**98.4** (**101**)	13.2	4.6	3.0	**25.9** (**29**)
	V15719	R	**45.9** (**50**)	**6.1** (**9**)	—	—	14.6
Pubis	V15939	R	—	—	—	3.7	—
	V12542	R	—	—	—	2.8	—
	V15719	R	—	—	5.6	—	—

TABLE A4. Measurements of the hand limb elements.

Bone	Specimen number	L/R	Le (DV)	Wp (ML)	Wp (AP)	Wd (ML)	Wm (ML/AP)	Lpf
Femur	V15939	R	132.1	38.1	—	36.1	13.2	60.2
	V15939	L	134.7	37.9	—	35.6	13.6	60.6
	V12529	L	90.6	**21**	—	18.9	8.5	37.6
	V12529	R	—	—	—	19.1	**8.4**	—
	V12542	R	94.4	22.6	—	19.1	**9.8**	43
	V12542	L	—	24.0	—	—	—	43.5
	V15719	L	49.6	10.1	—	—	4.9	20.9
	V15719	R	—	—	—	8.9	—	—
Tibia	V15939	R	161.4	—	32.8	34.4	8.9	—
	V15939	L	157.4	—	30.2	34.8	8.9	—
	V12529	R	107.8	—	21.2	21.4	7.7	—
	V12529	L	106.4	—	25.3	21.4	**7.7**	—
	V12542	R	113.4	—	**23.5**	23.4	**7.8**	—
	V15719	L	68.9	—	11.5	11.5	4.3	—
	V15719	R	65.3	—	11.4	11.5	4	—
Fibula	V15939	R	148.3	—	**16.6** (**20**)	11.3	4.3	—
	V15939	L	151	—	20.8	11.8	4.9	—
	V12529	R	101.3	—	13.2	6.2	2.4	—
	V12529	L	100.8	—	14.1	6.8	2.9	—
	V12542	R	100.1	—	—	—	**3.0**	—
	V15719	R	60.8	—	6.9	3	1.3	—

TABLE A5. Measurements of pedal elements.

				Proximal end		Distal end	
Specimen number	Bone	L/R	Le (AP)	Width (ML)	Height (DV)	Width (ML)	Height (DV)
V15939	Metatarsal I	L	43.6	2.9	9.4	8.0	7.4
	Phalange 1		15.3	8.8	9.0	7.7	6.9
	Phalange 2		18.2	6.9	7.8	—	—
	Metatarsal II		66.8	10.1	16.5	10.4	10.9
	Phalange 1		23.4	10.4	10.1	19.5	9.1
	Phalange 2		17.8	8.5	9.9	8.6	7.9
	Phalange 3		25.8	7.6	7.7	—	—
	Metatarsal III		76.2	8.9	15.3	13.5	9.5
	Phalange 1		18.0	11.1	9.7	10.3	8.1
	Phalange 2		18.0	8.5	10.3	8.2	7.0
	Phalange 3		11.7	7.4	8.1	6.8	6.2
	Phalange 4		30.7	8.0	8.1	—	—
	Metatarsal IV		67.1	14.5	12.5	10.0	10.2
	Phalange 1		16.9	9.5	9.5	9.9	6.9
	Phalange 2		13.1	8.7	9.0	8.7	6.7
	Phalange 3		11.8	8.6	8.7	8.4	6.4
	Phalange 4		10.8	7.7	8.3	8.2	6.7
	Phalange 5		21.9	7.9	8.3	—	—
	Metatarsal I	R	44.3	4.3	8.4	8.3	8.0
	Phalange 1		15.4	8.1	9.2	7.5	6.2
	Phalange 2		17.9	6.8	8.2	—	—
	Metatarsal II		69.1	9.2	20.3	10.3	9.0
	Phalange 1		21.8	10.4	10.2	8.9	8.0
	Phalange 2		15.5	8.7	9.3	7.4	6.8
	Phalange 3		24.5	6.8	7.6	—	—
	Metatarsal III		75.7	7.8	17.1	13.7	10.1
	Phalange 1		18.5	10.7	10.5	10.8	8.2
	Phalange 2		16.1	10.2	9.7	9.3	8.0
	Phalange 3		11.9	8.5	8.5	7.6	7.3
	Phalange 4		25.8	7.5	7.5	—	—
	Metatarsal IV		65.8	12.4	11.4	9.2	12.5
	Phalange 1		16.4	10.4	10.1	9.3	7.8
	Phalange 2		13.7	8.9	9.2	8.7	7.7
	Phalange 3		11.7	8.4	8.8	8.0	7.5
	Phalange 4		11.4	7.6	8.0	—	6.6
	Phalange 5		20.9	7.5	7.3	—	—
V12529	Metatarsal I	L	**13.7** (**25**)	1.0	3.8	—	—
	Metatarsal II		48.1	5.4	13.0	7.0	7.6
	Phalange 1		(**15.2**)	—	—	**6.6**	**6.6**
	Phalange 2		13.7	6.8	7.2	5.4	5.4

(Continued on next page)

TABLE A5. Measurements of pedal elements. *(Continued)*

Specimen number	Bone	L/R	Le (AP)	Proximal end		Distal end	
				Width (ML)	Height (DV)	Width (ML)	Height (DV)
	Phalange 3		16.7	5.5	5.6	—	—
	Metatarsal III		53.5	5.6	—	9.1	6.8
	Phalange 1		18.4	9.5	8.1	**(10)**	6.3
	Phalange 2		12.8	8.6	6.5	7.0	5.9
	Phalange 3		13.1	7.8	7.2	6.0	5.0
	Phalange 4		**16.2** (**18**)	5.9	5.5	—	—
	Metatarsal IV		47.6	8.2	8.6	5.7	6.7
	Phalange 1		11.9	7.9	7.2	5.7	5.7
	Phalange 2		10.0	4.5	7.0	(**5.0**)	5.1
	Phalange 3		9.1	—	6.6	—	4.7
	Phalange 4		8.1	—	6.2	—	4.3
	Phalange 5		13.8	4.6	4.8	—	—
	Metatarsal I	R	**22.5** (**25**)	—	—	4.8	4.6
	Phalange 1		11.1	5.9	5.7	4.9	4.3
	Phalange 2		—	4.3	4.9	—	—
	Metatarsal II		**41.5** (**49**)	—	—	6.0	7.9
	Phalange 1		16.4	6.4	7.6	5.3	5.7
	Phalange 2		13.3	—	7.7	—	4.6
	Phalange 3		**9.0** (**12**)	—	5.1	—	—
	Metatarsal III		54.1	7.2	—	9.0	6.6
	Phalange 1		17.6	9.3	7.8	7.8	6.4
	Phalange 2		12.7	8.0	7.8	6.9	5.9
	Phalange 3		6.8	6.1	7.3	7.0	6.2
	Phalange 4		16.7	4.4	6.8	0.0	0.0
	Metatarsal IV		**40.5** (**50**)	—	—	9.7	5.9
	Phalange 1		12.2	—	7.5	—	5.6
	Phalange 2		10.0	—	7.4	—	5.0
	Phalange 3		9.6	—	6.1	—	3.9
	Phalange 4		9.1	—	6.1	—	3.8
	Phalange 5		12.2	4.2	7.0	—	—
	Metatarsal V		**19.6**	2.8	6.8	—	—
V12542	Metatarsal II	R	50.2	—	—	7.8	—
	Phalange 1		17.0	**8.6**	—	7.4	—
	Metatarsal III		59.4	**8.0**	—	9.7	—
	Phalange 1		18.1	9.3		9.1	6.3
	Metatarsal IV		50.1	8.6	6.7	7.8	6.5
V15719	Metatarsal II	L	33.5	3.1	—	3.1	—
	Phalange 1		9.3	2.6	—	2.7	3.1
	Phalange 2		8.6	2.8	3.6	2.8	2.7
	Metatarsal III		37.8	3.7	5.4	4.8	3.7
	Metatarsal IV		**21.7** (**33**)	4.2	5.0	—	—
	Metatarsal I	R	19.9	—	—	2.9	2.5
	Metatarsal II		33.1	2.0	3.0	3.7	3.4
	Metatarsal III		36.0	3.0	—	4.5	3.6
	Metatarsal IV		31.5	4.6	—	4.0	4.0
	Phalange 1		8.1	4.0	3.4	3.0	2.9

APPENDIX 2. Updated character scores for *Jeholosaurus shangyuanensis*, *Koreanosaurus* (based on Huh et al., 2010), and *Yueosaurus* (based on Zheng et al., 2012), and additional scores for *Albalophosaurus*. The latter taxon was originally scored for inclusion in an expanded version of Butler et al. (2008) (see Ohashi and Barrett, 2009), whereas the most recent iteration of this phylogeny incorporates six new characters (characters 222–227; Butler et al., 2011), whose scores are provided here. Other scores for *Albalophosaurus* remain unchanged from those in Ohashi and Barrett (2009). The full data matrix used for the analysis conducted herein is available in Supplementary Information and the character list is published in Butler et al. (2011). Characters for *Jeholosaurus* whose scoring differs from that in Butler et al. (2011), following from the new data presented herein (mainly as the result of adding previously missing data), are shown in bold type: these account for changes in 52 character scores (23% of the total).

<Matrix>

	1	11	21	31	41
Jeholosaurus	0?0-11001	1010-00011	000??10?10	000100-000	1000010000
Koreanosaurus	??????????	??????????	??????????	??????????	??????????
Yueosaurus	??????????	??????????	??????????	??????????	??????????
	51	61	71	81	91
Jeholosaurus	0110000001	11010000-	0000100?00	?00**1??0**01	110**0**001000
Koreanosaurus	??????????	??????????	??????????	??????????	??????????
Yueosaurus	??????????	??????????	??????????	??????????	??????????
	101	111	121	131	141
Jeholosaurus	1101000000	001011?110	0-00001111	00**0**1??**300**	**00**?**0**?**1**??**10**
Koreanosaurus	??????????	??????????	??????????	???0??????	???????100
Yueosaurus	??????????	??????????	??????????	???0??????	00?0?????0
	151	161	171	181	191
Jeholosaurus	**01000**?????	???**0100000**	**0-11101100**	**00110110-**?	**01**???**1**0131
Koreanosaurus	10?01?????	????0???0??	????111?0?	??????????	??????0131
Yueosaurus	00?00?????	??????????	?????????0	?0???110??	?????10???
	201	211	221		
Jeholosaurus	2000011110	10--0**1**?**0**00	0??0001		
Koreanosaurus	200011????	??????0??00	0?000?1		
Yueosaurus	20???1????	????000?00	0??000?		

New scores for *Albalophosaurus*: character 222(1); characters 223–227 all '?'.